Scott E. R. D., Keil K., Goldstein J. I., Asphaug E., Bottke W. F., and Moskovitz N. A. (2015) Early impact history and dynamical origin of differentiated meteorites and asteroids. In *Asteroids IV* (P. Michel et al., eds.), pp. 573–595. Univ. of Arizona, Tucson, DOI: 10.2458/azu_uapress_9780816532131-ch030.

Early Impact History and Dynamical Origin of Differentiated Meteorites and Asteroids

Edward R. D. Scott and Klaus Keil
University of Hawai'i at Mānoa

Joseph I. Goldstein
University of Massachusetts (now deceased)

Erik Asphaug
Arizona State University

William F. Bottke
Southwest Research Institute

Nicholas A. Moskovitz
Lowell Observatory

Differentiated asteroids and igneous meteorites present numerous challenges to our understanding of the impact and dynamical evolution of asteroids and meteorite parent bodies. Igneous meteorites, including irons, achondrites, and stony-iron meteorites, testify to the prior existence of ~100 differentiated bodies. Destruction of these bodies by hypervelocity impact over 4 G.y. would have required numerous giant impacts, although this is inconsistent with the preservation of Vesta's basaltic crust and the lack of differentiated asteroid families. We review recent advances in elucidating the early chronology of meteorites, spectroscopic observations of likely differentiated asteroids, petrological studies of differentiated meteorites, impact disruption of differentiated planetesimals during accretion, and dynamical scenarios for capturing material into the asteroid belt. Together, these advances suggest a new paradigm in which planetesimals accreted rapidly in the inner solar system and were melted by ^{26}Al less than 2 m.y. after the formation of calcium-aluminum-rich inclusions (CAIs). While molten they were disrupted by grazing hit-and-run impacts during the accretion of planetesimals. Later, when still hot, the survivors were disrupted by hypervelocity impacts. Impact debris from the differentiated bodies was transferred from the newly formed terrestrial planet region to stable orbits in the asteroid belt. This evolutionary history leaves many questions unanswered but suggests new paths for future exploration of the asteroid belt and petrological and isotopic studies of meteorites.

1. INTRODUCTION

Laboratory studies of igneously formed meteorites suggest that numerous meteorite parent bodies were melted to form metallic cores and silicate mantles. Studies by the Dawn spacecraft confirm that (4) Vesta melted in this way (*McSween et al.,* 2013; see the chapter by Russell et al. in this volume). In principle, one would think the origin of iron and stony-iron meteorites and achondrites would be straightforward to investigate, but this is not the case. If disrupted Vesta-like differentiated bodies were once common in the main belt and they were the ultimate source of the differentiated meteorites, one might expect collisions to have created enormous numbers of V-type asteroids that were not derived from Vesta, as well as ample numbers of mantle and core fragments compared to the rest of the main-belt population. This is not observed. Instead, only limited examples of asteroids composed predominantly of core metallic Fe-Ni (possibly some M-type asteroids) or mantle olivine (some A-type asteroids) have been identified. Very few of these bodies are members of asteroid families, with those in families having orbits and sizes most consistent with being interlopers.

Differentiated asteroids and meteorites provide many other challenges to our understanding of the formation and evolution of the asteroid belt. How could core samples have been extracted from numerous large differentiated bodies when Vesta's basaltic crust was preserved (*Davis et al.,* 1985)? Where are the meteorites from the olivine-rich mantles of the parent bodies of the 12 groups of iron meteorites and the ~50–70 parent bodies of the ungrouped irons, the two groups of pallasites, and the type 4–6 ungrouped pallasites — "the great dunite shortage" (*Bell et al.,* 1989)? We also lack mantle and core samples from the parent asteroids of the angrites and the ungrouped eucrites like Northwest Africa (NWA) 011 and Ibitira (*Krot et al.,* 2014). Where is the missing Psyche family of silicate-rich asteroids (*Davis et al.,* 1999)? Why are meteorites derived from far more differentiated parent bodies than chondritic parent bodies even though the asteroid belt is dominated by C and S complex chondritic asteroids (*Bottke et al.,* 2006)?

We reassess ideas about the dynamical origin and early impact histories of differentiated asteroids and meteorites in the light of major advances since *Asteroids III*. These include advances in our understanding of the chronology of the early solar system, the distribution of short-lived isotopes including ^{26}Al, the identification of pristine chondrites and differentiated meteorites that escaped prolonged alteration or metamorphism, the thermal histories of differentiated meteorites, the nature of S asteroids, impact modeling during accretion, and dynamical studies of planetesimal accretion. Together, these advances suggest a new paradigm (*Bottke et al.,* 2006; *Goldstein et al.,* 2009) in which planetesimals accreted rapidly in the inner solar system and were rapidly melted by ^{26}Al less than 2 m.y. after CAI formation. While they were still molten or semimolten, planetesimals were disrupted — first by grazing impacts during the accretion that harvested the objects making slow, direct hits (*Asphaug et al.,* 2006), and later by hypervelocity impacts when larger bodies excited their orbits. Impact debris from the differentiated bodies was tossed into the asteroid belt. Most iron meteorites did not cool slowly inside insulating silicate mantles, like Vesta's core, but rapidly with little or no silicate insulation less than 5 m.y. after CAI formation. In this scenario, Vesta — the dominant single source of differentiated meteorites, viz., the howardites, eucrites, and diogenites (HEDs) — is not a typical differentiated asteroid.

In this chapter, we first describe the isotopic evidence that has been used to establish a new chronology for melting and solidification of igneous meteorites and to identify the heat source. Then we review the types, properties, and abundances of differentiated asteroids and asteroid families. Next, we describe the various types of igneous meteorites, focusing on evidence that their parent bodies were disrupted by impacts while they were still partly or wholly molten. Finally, we discuss numerical simulations of grazing impacts between differentiated planetesimals during accretion ("hit-and-run" impacts), and dynamical studies that suggest how planetesimals could have been scattered into the asteroid belt from 1 to 2 AU.

2. MELTING AND SOLIDIFICATION OF ASTEROIDS

2.1. When Were Meteoritic Bodies Melted and Solidified?

Advances in the use of short-lived and long-lived radionuclides for dating meteorites since *Asteroids III* have revolutionized our understanding of the timescales for early solar system processes (*Davis and McKeegan,* 2014). The U-Pb system provides two isotopic clocks with different half-lives: ^{238}U decays to ^{206}Pb with a half-life of 4469 m.y., and ^{235}U decays to ^{207}Pb with a half-life of 704 m.y. Measurements of ^{207}Pb/^{204}Pb and ^{206}Pb/^{204}Pb can provide ages with precisions of 0.1–1 m.y. in favorable cases. After allowance for small variations in the ^{238}U/^{235}U ratio (*Wadhwa,* 2014), the Pb-Pb technique gives ages of 4567.2 to 4568.2 Ma for CAIs from CV3 chondrites, which provide our best estimate of the formation age (t_0) of the first solid materials in the solar system. Figure 1, which shows ages of early solar system materials, was constructed using a mean value of 4567.5 Ma for t_0. [The small difference between this value and that preferred by *Davis and McKeegan* (2014) of 4567.3 ± 0.2 Ma from *Connelly et al.* (2012) is of no consequence in this discussion.]

Short-lived chronometers like ^{26}Al, which decays to ^{26}Mg with a half-life of 0.71 m.y., and ^{182}Hf, which decays to ^{182}W with a half-life of 8.90 m.y., provide relative ages. For example, CAIs have inferred initial ratios of ^{26}Al/^{27}Al that are roughly 8 (= 2^3)× higher than most chondrules, and so formed about 2 (3 × 0.71) m.y. before chondrules. Manganese-53, which decays to ^{53}Cr with a half life of 3.7 m.y., also provides valuable relative ages but cannot be used to date CAIs because Mn is depleted in CAIs and Cr shows mass-independent isotopic anomalies. The short-lived and long-lived chronometers are cross-calibrated using angrites — achondrites that crystallized 4–11 m.y. after CAIs and escaped extensive metamorphism and shock heating (*Brennecka and Wadhwa,* 2012; *Kleine et al.,* 2012). The oldest, fine-grained angrites such as D'Orbigny are especially important anchors for the short-lived chronometers as they crystallized and cooled very rapidly (in days).

Radioactive isotopic systems record the time at which diffusion of the parent and daughter isotopes between minerals effectively ceased. Thus ages of slowly cooled rocks depend on cooling rates (*Ganguly and Tirone,* 2001). Many igneous and metamorphosed meteorites cooled slowly at around 10–10^3°C m.y.$^{-1}$, so that radiometric ages based on isotopic systems in various minerals with closure temperatures that range from ~300° to 1100°C could differ by ~50 m.y. or more for slowly cooled meteorites, but only ~1 m.y. for quickly cooled meteorites. For example, Hf-W closure temperatures for pyroxene are ~750°–900°C, depending on grain size and cooling rate (*Kleine et al.,* 2008). However, zircons may crystallize from melts above their Hf-W closure temperatures and so record the time of crystallization. Closure temperatures for Pb-Pb ages of phosphates in or-

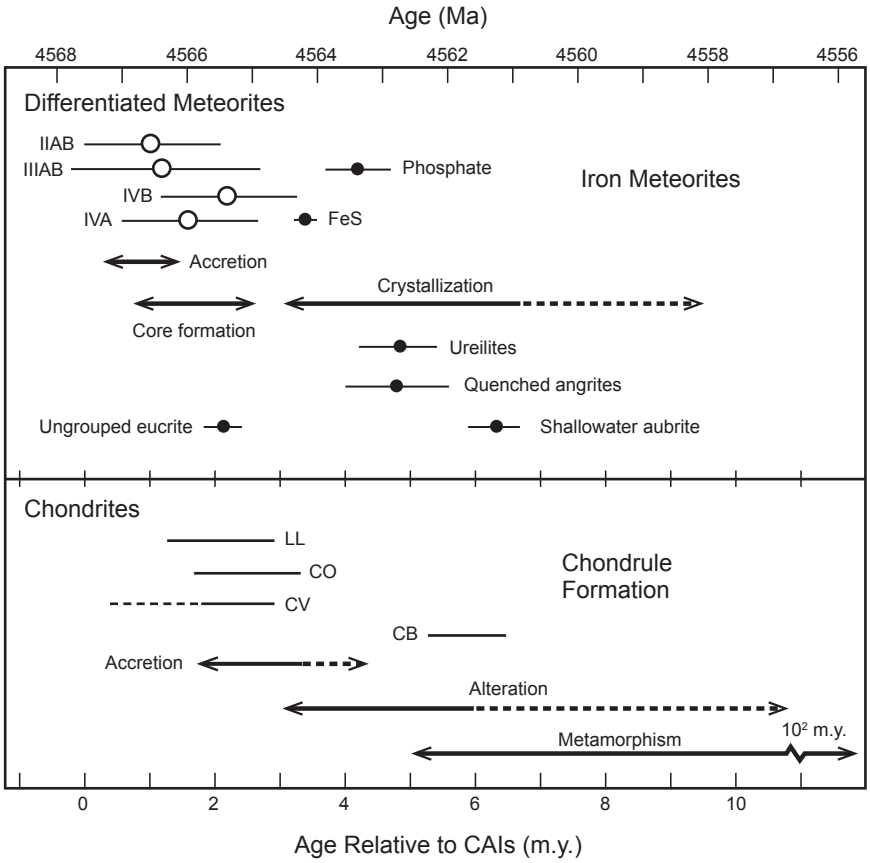

Fig. 1. Chronology of differentiated meteorites and chondrites inferred from their radiometric ages. Core formation ages of the IIAB, IIIAB, IVA, and IVB iron meteorite parent bodies are 1–2 m.y. after the CAI formation age, which is 4567.5 Ma. Their parent bodies probably accreted 0.5 to 1.5 m.y. after CAIs. Ages of phosphate and troilite in iron meteorites, ureilites, quenched angrites, the ungrouped eucrite, Asuka 881394, and the Shallowater aubrite indicate crystallization and cooling within 2–7 m.y. of CAIs. Ages of chondrules in the least-metamorphosed LL, CO, and CV chondrites, which are shown by horizontal lines, suggest that the parent bodies of most chondrites accreted later than the differentiated asteroids — around 2–3 m.y. after CAI formation. The metal-rich CB chondrites accreted much later, at around 5 m.y. after CAIs. Alteration and metamorphic minerals in chondrites formed 5–100 m.y. after CAIs. Dashed lines indicate less common features. (See text for sources of data.)

dinary chondrites range from ~500° to ~750°C depending on the cooling rate (*Ganguly et al.,* 2013), whereas closure temperatures for Pb-Pb ages of pyroxene are ~700°–900°C (*Amelin et al.,* 2005).

Radiometric ages based on the ^{182}Hf-^{182}W, ^{26}Al-^{26}Mg, and ^{53}Mn-^{53}Cr isotopic records for angrites and CAIs are reasonably concordant with the Pb-Pb ages showing that all three short-lived isotopic systems are robust chronometers (*Kleine et al.,* 2013; *Kruijer et al.,* 2014). However, small but significant discrepancies between isotopic chronometers require further study (*Davis and McKeegan,* 2014). Because of the major advances in the four radiometric dating systems described above and the discovery of pristine chondrites and achondrites that largely escaped alteration, metamorphism, or impact processing after their formation, we now have a radically new chronology for the inner solar system. Figure 1 summarizes various ages of differentiated meteorites and chondrites and their components based on these four chronometers.

Key evidence that differentiated planetesimals formed soon after CAIs and before the chondrite parent bodies comes from Hf-W isotopic measurements of chondrites, CAIs, and differentiated meteorites (*Kleine et al.,* 2005). Deviations in the ^{182}W/^{184}W ratio in parts per 10^4, which are called ε^{182}W values, can be attributed to separation of metal and silicate when ^{182}Hf was still decaying to ^{182}W because tungsten is siderophile (metal-loving) whereas hafnium is lithophile (silicate-loving). The ε^{182}W values of most iron meteorites were fixed when molten metal segregated into metallic cores as the radioactive ^{182}Hf was retained in the silicate and are

very close to the inferred initial $\varepsilon^{182}W$ value in CAIs. Figure 1 shows that core formation ages inferred from $\varepsilon^{182}W$ values for four groups of iron meteorites, IIAB, IIIAB, IVA, and IVB, range from 1.0 to 2.2 m.y. after CAIs (*Kruijer et al.,* 2012, 2013).

Additional isotopic evidence for the early accretion of differentiated planetesimals comes from high-precision Mg isotopic measurements of achondrites (*Bizzarro et al.,* 2005; *Davis and McKeegan,* 2014). For example, *Baker et al.* (2012) used this technique to infer that the parent body of the main-group pallasites differentiated 1.2 ± 0.3 m.y. after CAIs. The oldest achondrite, Asuka 881394, which is an ungrouped eucrite, crystallized 2 m.y. after CAIs according to Pb-Pb, Al-Mg, and Mn-Cr isotopic constraints (Fig. 1) (*Wadhwa et al.,* 2009). Virtually all vestan eucrites cannot be dated using these techniques, probably because of extensive thermal processing after they crystallized.

Contrary to the expectations of many workers, the new chronology shows that chondrites are not derived from the first generation of planetesimals. Ages of most chondrules based on ^{26}Al-^{26}Mg and Pb-Pb isotopic systems are 1.5–2.5 m.y. after CAIs (Fig. 1) (*Kita and Ushikubo,* 2012; *Wadhwa,* 2014). These ages are consistent with formation of chondrules by splashing when largely molten planetesimals collided at low speed during accretion (*Asphaug et al.,* 2011; *Sanders and Scott,* 2012). Since chondrite accretion postdates the formation of the constituent chondrules, most chondrites accreted 2–3 m.y. after CAIs. Although the origin of most chondrules remains uncertain, chondrules in the metal-rich CB chondrites have unique isotopic and chemical signatures indicating that they probably formed in a giant impact that created melt droplets and vapor condensates ~5–6 m.y. after CAIs (*Krot et al.,* 2005, 2010).

2.2. Heat Source for Melting

Isotopic data from meteorites provide strong evidence that ^{26}Al was the most potent heat source for melting planetesimals in the early solar system. Two other short-lived nuclides, ^{10}Be and ^{36}Cl, which were not uniformly distributed in the solar system, formed in a late-stage irradiation, but this was insufficient to account for the abundance of ^{26}Al. An external source is therefore required for this nuclide — probably the winds from a massive star prior to its explosion (*Davis and McKeegan,* 2014). Some rare CAIs with large isotopic anomalies of nucleogenetic origin appear to have formed before ^{26}Al was homogenized in the disk by radial mixing (*Krot et al.,* 2012). However, the concordance between isotopic chronometers described above suggests that ^{26}Al was quickly homogenized. The initial $^{26}Al/^{27}Al$ ratio of 5.2×10^{-5} in CAIs can therefore be used to estimate the heating energy available in dry chondritic material due to the decay of ^{26}Al (Fig. 2) (*Sanders and Scott,* 2012). At the time that most CAIs were formed (t_0), 6.6 kJ g^{-1} of heat was available from ^{26}Al decay, which is about four times larger than the 1.6 kJ g^{-1} needed to melt dry chondritic dust in the insulated interior of a planetesimal (*Sanders and Scott,* 2012). Thus well-insulated planetesimals with radii of more than 20 km that accreted less than 1.5 m.y. after CAIs (about two half-lives of ^{26}Al) were melted. Bodies that accreted soon afterward were heated but not melted. It is likely that ^{26}Al was also the dominant heat source for alteration on wet asteroids, as most well-dated alteration minerals in carbonaceous chondrites formed 3–6 m.y. after CAIs (*Sugiura and Fujiya, 2*014; see also the chapter by Krot et al. in this volume). For further details on the thermal modeling of melted planetesimals, see *Hevey and Sanders* (2006), *Moskovitz and Gaidos* (2009), *Sanders and Scott* (2012), and *Neumann et al.* (2012).

Although ^{60}Fe has been considered as a second possible source of radioactive heat, the current best estimate for the solar system initial $^{60}Fe/^{56}Fe$ ratio of $(1.0 \pm 0.3) \times 10^{-8}$ indicates that heating from ^{60}Fe decay would have been negligible (<20 K increase in temperature) (*Tang and Dauphas,* 2012). Alternative heating mechanisms such as electromagnetic induction do not appear to have played a major role in heating asteroids (e.g., *Marsh et al.,* 2006). Impacts cannot cause global heating and melting of asteroids, even very porous ones (*Keil et al.,* 1997). Nevertheless, impacts into highly porous targets can cause localized heating, which may have played a role in the formation of certain igneous meteorites like IAB and IIE irons (*Davison et al.,* 2012, 2013; *Ciesla et al.,* 2013; *Wasson and Kallemeyn,* 2002). In addition, the Portales Valley H chondrite, which contains centimeter- to millimeter-wide metallic veins with a Widmanstätten pattern like iron meteorites, probably formed by impact heating or impact-induced frictional heating of a hot target (*Kring et al.,* 1999; *Rubin et al.,* 2001).

3. DIFFERENTIATED ASTEROIDS

Asteroid compositions have traditionally been established via spectroscopic observations at visible and near-infrared wavelengths (*Burbine,* 2014). Feature-based taxonomic systems (e.g., *DeMeo et al.,* 2009) allow mapping of spectral classes to broadly defined compositional groups, while detailed modeling of mineral absorption features can yield specific compositional information (see the chapter by Reddy et al. in this volume). Asteroids derived from igneously differentiated parent bodies range from those with prominent absorption features and reasonably constrained compositions (e.g., V-types), to those that are challenging to characterize due to muted or absent absorption features (e.g., M-types). Here we focus on asteroids that may have been heated to high enough temperatures to melt or partially melt silicate or metal-sulfide (>950°C and >1050°C respectively) and to mobilize these melts. We exclude asteroids like (1) Ceres that may have experienced silicate-water differentiation (see the chapter by Rivkin et al. in this volume).

3.1. Basaltic Crust: V-Types

Named after their archetype, the 530-km-diameter (4) Vesta, V-type asteroids have long been spectroscopically

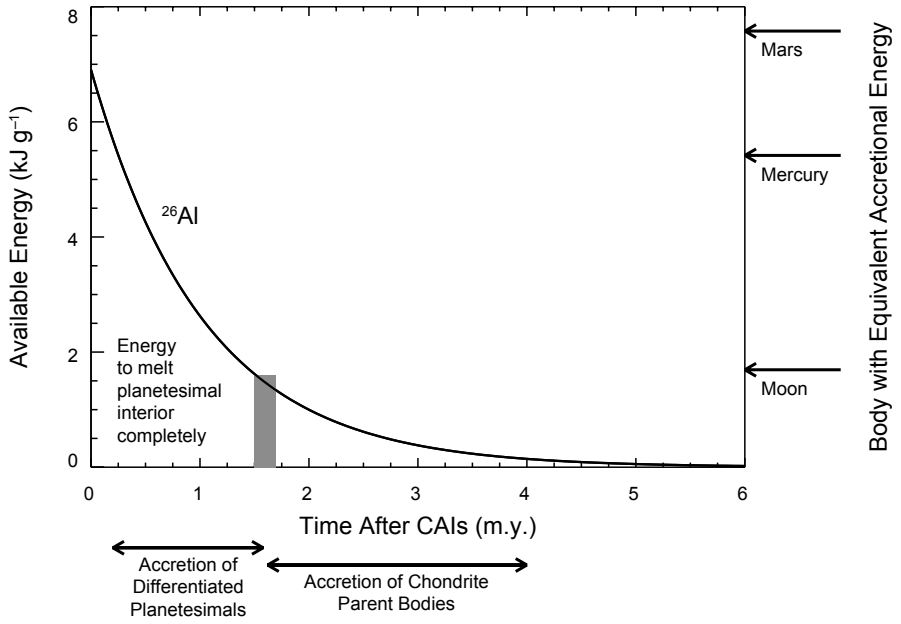

Fig. 2. Available thermal energy from ^{26}Al decay in dry chondrites as a function of time since CAI formation (after *Sanders and Scott,* 2012). Differentiated planetesimals accreted within 1.6 m.y. of CAI formation when the available energy from ^{26}Al exceeded 1.6 kJ g^{-1}, which is the energy needed to melt a chondrite completely. The parent bodies of nearly all chondrites accreted 1.6–4 m.y. after CAIs formed (see Fig. 1). The righthand axis shows the equivalent accretional energy (or gravitational binding energy) of the Moon, Mercury, and Mars.

linked to the basaltic HED meteorites (*McCord et al.,* 1970; *Consolmagno and Drake,* 1977; *Cruikshank et al.,* 1991; *Binzel and Xu,* 1993; *Burbine et al.,* 2001; *McSween et al.,* 2013). Compositional analyses support this link (*Duffard et al.,* 2004; *Mayne et al.,* 2011; *De Sanctis et al.,* 2011). V-type asteroids, apart from Vesta, are small, <10 km in diameter, and the vast majority of V-types are part of the Vesta asteroid family, which spans the inner main belt between the ν_6 secular resonance along the inner main belt's periphery at 2.1–2.3 AU (depending on inclination) and the 3:1 mean-motion resonance with Jupiter near 2.5 AU (*Carruba et al.,* 2005; *Nesvorny et al.,* 2008; *Moskovitz et al.,* 2010; see also the chapter by Nesvorny et al. in this volume). Most of the Vesta family probably stems from the impact events that made the 500-km basin Rheasilvia, with a crater retention age of ~1 Ga, and the 400-km basin Veneneia, with a crater retention age of >2 Ga (*Marchi et al.,* 2012; see also the chapter by Marchi et al. in this volume).

Several examples of non-Vesta V-type asteroids have been discovered in the middle and outer main belt beyond 2.5 AU (*Lazzaro et al.,* 2000; *Roig et al.,* 2008; *Moskovitz et al.,* 2008; *Duffard and Roig,* 2009; *Solontoi et al.,* 2012). These V-types are dynamically separated from Vesta by one or more of the Kirkwood gaps and show a wide range in semimajor axis, eccentricity, and inclination. They are therefore unlikely to have been dynamically transported from the Vesta family to their current locations and are probably composed of fragments from other Vesta-like bodies (e.g., *Nesvorny et al.,* 2008). In a few cases, compositional analyses suggest that these outer-belt V-types are compositionally distinct from Vesta and the vestoids (*Hardersen et al.,* 2004; *Burbine,* 2014).

3.2. Olivine-Rich Mantle: A-Types

The spectra of A-type asteroids closely resemble those of olivine-dominated compositions, with slope differences potentially due to the effects of space weathering (e.g., *Hiroi and Sasaki,* 2001). Some A-types have magnesian olivine compositions consistent with differentiation of ordinary chondrites; others contain ferroan olivine like that found in R-chondrites or igneous differentiates from R-chondrite-like parent bodies (*Sunshine et al.,* 2007; *Burbine,* 2014). A-types with magnesian compositions tend to be olivine-rich (~70–90% abundance) with small amounts of pyroxene that produce subtle 2-μm absorption features, whereas the ferroan A-types have spectra consistent with a monomineralic interpretation, i.e., no 2-μm band (*Sanchez et al.,* 2014). A-type asteroids and their meteoritic counterparts (e.g., pallasites, brachinites, R-chondrites) are rare.

If the asteroid belt had been composed largely of highly reduced meteorites like enstatite chondrites and achondrites, which have virtually no Fe^{2+}, the apparent lack of meteorites and asteroids composed mainly of olivine would be

understandable, as chondrites have atomic Mg/Si ratios of around 1, like enstatite ($MgSiO_3$). However, most meteorites and asteroids are much more oxidized with significant concentrations of Fe^{2+}, so we should expect differentiated bodies to contain major amounts of olivine $(Mg,Fe)_2\ SiO_4$. We discuss the dearth of dunite in section 7.

3.3. Metal-Rich: Some M-Types

M-types have traditionally been linked to iron meteorites. An M-type classification is not exclusively a spectroscopic designation, but instead requires knowledge of albedo (10–30%) to distinguish their largely featureless spectra from others within the broad X-complex (*Tholen,* 1984). Focused studies have suggested that additional information like high radar albedo (*Shepard et al.,* 2010), spectral observations around 3 μm to look for signatures of hydrated minerals (*Rivkin et al.,* 2000; see also the chapter by Rivkin et al. in this volume), and near-infrared continuum curvature (*Clark et al.,* 2004) can be used to further distinguish metal-rich M-types from other spectrally degenerate asteroids. However, it is unclear what fraction of taxonomic M-types are truly metal-rich. Most of the M-types that are inferred to be metal-rich from radar studies also show 1- and 2-μm silicate spectral features (*Ockert-Bell et al.,* 2010). *Neeley et al.* (2014) found that for one-third of the Xc and Xk objects, the best spectral match was an iron meteorite; one-fifth were matched best by E chondrites. Xk-type asteroids have also been linked with mesosiderites (*Vernazza et al.,* 2009).

The largest of the iron-rich M-types, which is (16) Psyche, with dimensions of 240 × 185 × 145 km, possibly came from a Vesta-sized differentiated body that completely lost its crust/mantle silicates via one or more hit-and-run collisions (see section 5). (216) Kleopatra is another canonical M-type but has a relatively low density of 3600 ± 400 kg m^{-3} (*Descamps et al.,* 2011), suggesting it may be a highly porous collection of collisionally evolved core fragments.

3.4. Chemically Reduced Crust: E-Types

The E-type asteroids are also a part of the X-complex and are distinguished by a high albedo, >30%. These properties are consistent with a link to aubrites, igneous enstatite-rich meteorites that formed in chemically reducing conditions. This link to aubrites is consistent with compositional interpretations of the Rosetta mission target asteroid (2867) Šteins (e.g., *Barucci et al.,* 2008). E-types are scattered within the inner main belt, but they dominate the Hungaria region ($1.78 < a < 2.0$ AU, $e < 0.18$, $16° < i < 34°$) and are associated specifically with the Hungaria family (*Warner et al.,* 2009; *Milani et al.,* 2010). These asteroids may represent the best available analogs to the precursor material from which the terrestrial planets formed. It is also possible that they were an important source of impactors on Earth during the late heavy bombardment (*Bottke et al.,* 2012; see also the chapter by Morbidelli et al. in this volume).

3.5. Melt Byproducts: S-Complex

Most S-type asteroids are probably composed of ordinary chondrite material (*Vernazza et al.,* 2014; see also the chapter by Vernazza et al. in this volume) rather than differentiated material (e.g., *Bell et al.,* 1989). However, several subclasses within the S-complex (e.g., Sv, Sa, Sr) may be linked to fully or partially differentiated parent bodies (*Burbine,* 2014). Compositional analysis of several of the largest members in the Merxia and Agnia S-type families, as well as asteroid (17) Thetis, suggest that their ratio of high-calcium pyroxene to total pyroxene is greater than ~40% (*Sunshine et al.,* 2004). Among meteorites, only the eucrites have such high values, suggesting that these S-types may have experienced a history consistent with igneous activity. However, *Vernazza et al.* (2014; see also the chapter by Vernazza et al. in this volume) find that the Merxia and Agnia asteroid families are likely parent asteroids of H chondrites.

Compositional analyses of the S-type near-Earth object (1036) Ganymed and the main-belt family associated with (170) Maria suggest that these objects may be collisional agglomerations of basalt and metal analogous to mesosiderites (*Fieber-Beyer et al.,* 2011a,b). This raises the interesting possibility that highly collisionally evolved differentiated asteroids could be masquerading as S-type asteroids (see the chapter by Vernazza et al. in this volume).

3.6. Spectral End Members and Partial Differentiation

Two objects stand out as the only known members of their respective taxonomic classes: the O-type asteroid (3628) Božněmcová and the R-type asteroid (349) Dembowska. Compositional interpretations of these unusual objects have been varied and include putative links to the angrites in the case of Božněmcová (*Cloutis et al.,* 2006) and some form of pyroxene-olivine melt or melt residual in the case of Dembowska (*Burbine,* 2014). Neither of these objects have good spectral analogs among meteorites or terrestrial samples.

The K-type taxonomic class has also seen varied compositional interpretations. Both the Eos family (*Mothe-Diniz and Carvano,* 2005; *Mothe-Diniz et al.,* 2008) and the Eunomia family (*Nathues et al.,* 2005; *Nathues,* 2010) have been linked to partially differentiated parent bodies.

However, alternative interpretations suggest a link to nondifferentiated CO and CK carbonaceous chondrites (e.g., *Clark et al.,* 2009). The asteroid (21) Lutetia may be a partially differentiated asteroid with a metallic core and a chondritic crust (*Weiss et al.,* 2012; *Weiss and Elkins-Tanton,* 2013), although this is a point of some debate (*Barucci et al.* 2012; see also the chapter by Barucci et al. in this volume).

3.7. Abundance of Differentiated Asteroids

Figure 3 shows the orbital distribution of the differentiated V-, A-, and E-type taxonomic classes relative to the

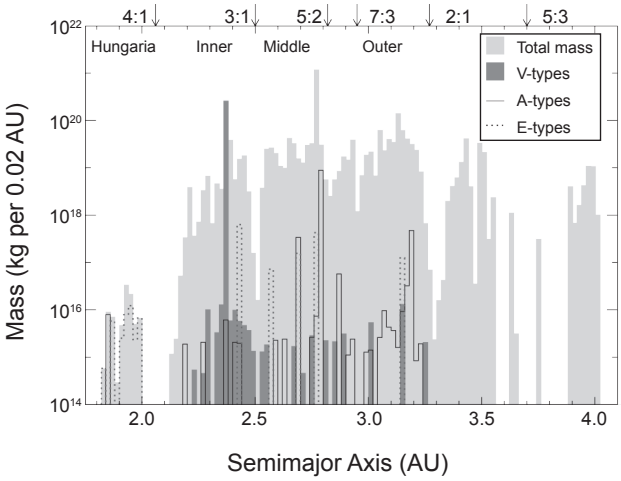

Fig. 3. Distribution by mass of differentiated asteroids as a function of their semimajor axis (data from *DeMeo and Carry,* 2013). M-types are omitted due to uncertainty in the identification of metallic varieties. Differentiated asteroids are relatively small, aside from Vesta, and have semimajor axes from 1.8 to 3.3 AU.

total mass in the asteroid belt (from *DeMeo and Carry,* 2013, 2014). Accounting for all the previously discussed taxonomic types and asteroid families that are associated with igneous histories, the mass of differentiated material among observed bodies is only ~15–20% of the total mass in the main belt, with Vesta alone accounting for ~10%. Table 1 summarizes some of the largest examples of fully differentiated asteroids, including (1459) Magnya, which is the largest V-type asteroid not related to Vesta. The masses in this table are either referenced or were computed assuming mean densities for the respective taxonomic classes (*DeMeo and Carry,* 2013) and diameters as given.

Differentiated asteroid families are surprisingly scarce. Only four (Hungaria, Vesta, Merxia, and Agnia) of the currently known 76 asteroid families (*Masiero et al.,* 2013) have been linked (or tentatively linked) to fully differentiated parent bodies. Another two (Eos, Eunomia) have been connected to partially differentiated precursors. However, no known asteroid family contains the crust, mantle, and core fragments expected from a differentiated parent body. The majority of other differentiated asteroids are isolated objects with no associated collisional families, likely representing relic fragments of now fully eroded parent bodies.

Since family members are composed of fragmental debris, it might be argued that they are "camouflaged," namely covered with small debris that reaccreted immediately after the family-forming event (e.g., see *Michel et al.,* 2004). However, spacecraft flybys of (951) Gaspra, part of the Flora family, and (243) Ida, part of the Koronis family, provide no compelling evidence that their subsurface materials, revealed via numerous impact craters, are different from the surface material (*Farquhar et al.,* 2002).

The lack of differentiated asteroids and families is surprising in light of the large number (~50–100) of distinct differentiated parent bodies represented by the iron meteorites (section 4). If differentiation was so common, where are the asteroidal relics of this process? This long-standing paradox is most pronounced for differentiated mantle material, which is quite rare among both asteroids and meteorites (*Chapman,* 1986; *Bell et al.,* 1989; *Burbine et al.,* 1996).

4. DIFFERENTIATED METEORITES

4.1. Types of Differentiated Meteorites

Differentiated meteorites formed by melting and crystallization in planetesimals with bulk compositions that were near solar, or chondritic, except for their volatile contents. For bodies that experienced low degrees of melting, the products resemble ultrametamorphosed chondrites or residues from low degrees of partial melting and have been called "primitive achondrites" (e.g., *Krot et al.,* 2014). For bodies that were largely molten, the igneous products are grossly different from chondrites in their mineralogy and chemical composition. Metallic Fe-Ni and troilite (FeS) formed molten cores from which most iron meteorites appear to have been derived. Silicates formed basaltic crusts and olivine-rich and pyroxene-rich mantles that supply us with achondrites. Impacts created a third type of differentiated meteorite — stony irons — by mixing metal and silicate in roughly equal proportions. Two major types of stony-irons are known. Pallasites are made of Fe-Ni from molten cores that were mixed with fragments of olivine mantles. Mesosiderites are mixtures of molten metal, basalts, and gabbros, and impact melted silicates, with little olivine. The properties of the major types of differentiated meteorites and their fall

TABLE 1. Examples of the largest asteroids within differentiated asteroid classes.

Object	Type	Mass (kg)	Diameter (km)	Inferred composition	References
(4) Vesta	V-type	2.59e20	525.4	Basaltic surface, fully differentiated	*McSween et al.* (2013)
(434) Hungaria	E-type	2.6e15	11	Enstatite-rich, aubrite	*Shepard et al.* (2008)
(354) Eleonora	A-type	8.8e18	165	Olivine mantle	*Masiero et al.* (2011)
(1459) Magnya	Non-Vesta V-type	4.9e15	17	Basaltic crust	*Delbo et al.* (2006)
(16) Psyche	M-type	2.7e19	248	Metallic core material	*Carry* (2012)
(216) Kleopatra	M-type	4.64e18	127	Metallic core material	*Descamps et al.* (2011)

frequencies are summarized in Table 2. Chemical and isotopic data suggest that each type of differentiated meteorite probably comes from a separate body. Winonaites and IAB irons are exceptions as they are genetically related and probably come from the same body.

Below we review the evidence that early impacts were involved in the formation of differentiated meteorites and the constraints on the timing, nature, and speed of the impacts.

4.2. Iron Meteorites

Iron meteorites are composed very largely of Fe with 5–60% Ni (mostly 5–10% Ni) with a few volume percent of troilite (FeS), phosphide ($(Fe,Ni)_3P$), and smaller amounts of chromite, carbides, phosphates, and other minerals (*Goldstein et al.,* 2009; *Benedix et al.,* 2014; *Krot et al.,* 2014). Minor and trace amounts of siderophile elements such as Ni, Co, P, Ga, Ge, Ir, Au, As, and W provide important clues to their origin. Moderately volatile elements like Ga and Ge vary enormously in their abundance: Ge/Ni ratios, for example, range from chondritic proportions (0.1–1× CI chondrites) to 10^{-4} of chondritic values. Depletion of volatiles reflects either early accretion in a hot solar nebula or volatile loss during impacts. Germanium concentrations in irons cluster into 14 groups, each of which contains between 5 and ~250 iron meteorites. Other elements like Au (Fig. 4b) and Ir show wide ranges within most groups, which approach the total range shown by all iron meteorites. Since concentrations of the nine major siderophile elements vary systematically within each group, there is little ambiguity in classifying meteorites into groups and locating each meteorite within its group. Mineralogical and isotopic data confirm that group members are closely related and probably formed in a single body. About 15% of irons have compositions that lie outside those of the groups and are called ungrouped irons. A few small, rapidly cooled and S-rich ungrouped irons probably formed by impact melting in ordinary chondrite bodies, e.g., Sahara 03505 (*D'Orazio et al.,* 2009). However, the remaining ungrouped irons appear to be derived from ~50 to 60 separate bodies (*Goldstein et al.,* 2009).

TABLE 2. Classification of differentiated meteorites.

Name	Fall freq.* (%)	Minerals†	Origin	References
Iron meteorites	4.3			
Groups IIAB, IIIAB, IVA, IVB, etc.	3.2	Metallic Fe-Ni, troilite (FeS)	Fractionally crystallized cores	*Goldstein et al.* (2009)
Groups IAB and IIE	1.1	Fe-Ni with silicate inclusions	Metallic pools in partly melted bodies	*Ruzicka* (2014)
Stony irons				
Pallasites	0.27	Fe-Ni, olivine ($Fa_{10–20}$)	Breccias of core and mantle formed in several bodies	*Yang et al.* (2010a), *Benedix et al.* (2014)
Mesosiderites	0.6	Fe-Ni, pyroxene ($Fs_{10–20}$), plagioclase ($An_{50–80}$)	Impact mixtures of basalt, gabbro, and Fe-Ni-S from a Vesta-like body	*Benedix et al.* (2014)
Achondrites				
Howardites, eucrites, diogenites	5.5	Pyroxene ($En_{14–79}$ $Wo_{2–5}$), plagioclase ($An_{73–93}$), silica	Breccias of basalts, gabbros, and pyroxenites from Vesta	*McSween et al.* (2013)
Angrites	0.09	Al-Ti- diopside ($Fs_{12–50}$), Ca-olivine, anorthite ($An_{86–100}$)	Oldest basaltic meteorites from a fully differentiated asteroid	*Keil* (2011)
Aubrites	0.8	Enstatite ($Fs_{0.1}$), minor plag, ol	Igneous rocks: mostly breccias	*Keil* (2010)
Ureilites	0.5	Ol ($Fo_{74–95}$), pyx (mostly $En_{68–87}$ $Wo_{2–16}$), graphite	Partial melt residues from which basalts were removed	*Goodrich et al.* (2004)
Primitive achondrites				
Brachinites	<0.1	Ol ($Fo_{64–73}$), pyx ($En_{40–63}$ $Wo_{36–48}$), plag ($An_{15–33}$)	Partial melt residues from FeO-rich body	*Keil* (2014)
Acapulcoites and lodranites	0.09	Ol ($Fo_{87–97}$), pyx ($En_{88–93}$ $Wo_{2–3}$ and $En_{50–54}$ $Wo_{43–46}$), Fe-Ni-S, plag ($An_{12–31}$)	Low-degree partial melting residues in one body	*Krot et al.* (2014)
Winonaites	0.09	Ol ($Fa_{1–4}$), pyx ($Fs_{1–9}$), plag ($An_{8–25}$)	Metamorphosed chondrites from IAB body	*Krot et al.* (2014)

* Source: Meteoritical Bulletin Database (*http://www.lpi.usra.edu/meteor/metbull.php*).
† Abbreviations: ol = olivine, pyx = pyroxene, plag = plagioclase; Fa= fayalite mol.%; Fs = ferrosilite mol.%; Wo = wollastonite mol.%; An = anorthite mol. %.

Not listed are the ungrouped irons (~100), ungrouped pallasites (~5), and ungrouped achondrites (≈50).

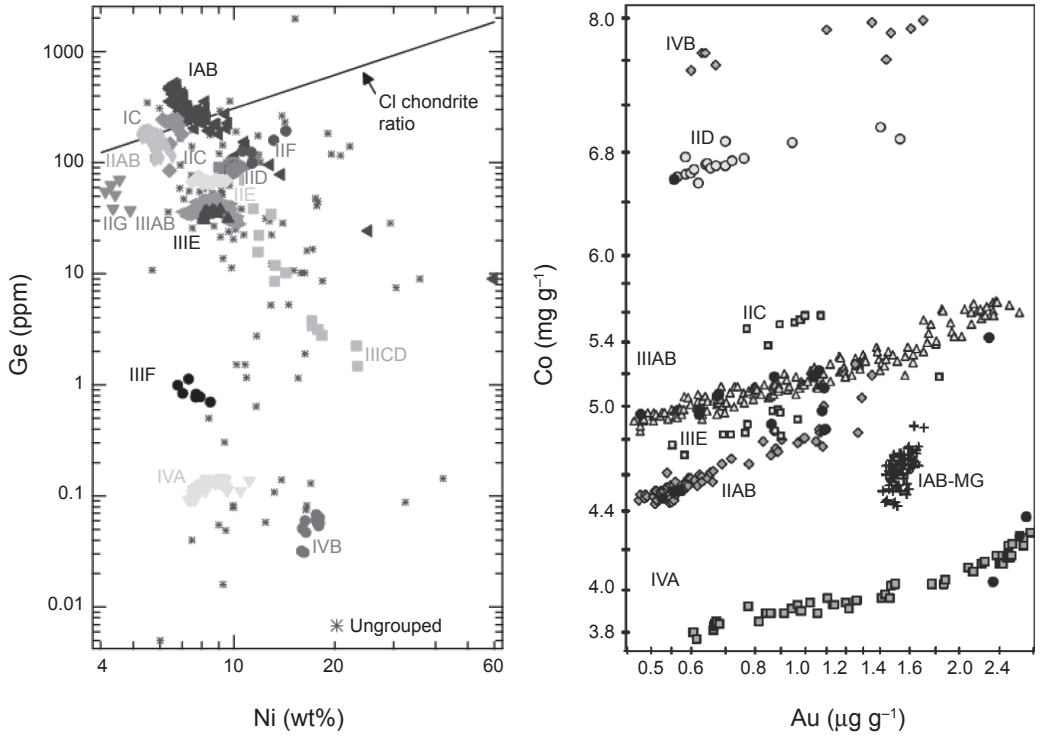

Fig. 4. Logarithmic plots showing the bulk compositions of iron meteorites. **(a)** Ge vs. Ni for grouped and ungrouped iron meteorites. Reproduced from *Goldstein et al.* (2009) by permisssion; image courtesy N. Chabot. **(b)** Co vs. Au for seven major groups of irons, which are thought to be derived from asteroidal cores that fractionally crystallized, and the group IAB-MG, which is rich in silicates and shows very different chemical trends. Reproduced from *Wasson* (2011) by permission.

Except for groups IAB, IIE, and IIICD, which show very different chemical trends from the other groups, chemical variations within each group can be explained by fractionation between solid and liquid Fe-Ni during solidification of a single large metallic magma, probably core material from a melted asteroid (*Chabot,* 2004; *Goldstein et al.,* 2009). The elements Au, As, Ni, Co, and P prefer liquid to solid Fe-Ni, whereas Ir, Re, and Os are concentrated preferentially in the solid, and Ge and Ga are scarcely fractionated. Chemical trends in fractionally crystallized groups, which are sometimes called "magmatic groups," are largely consistent with those calculated using fractional crystallization models and experimentally determined solid-liquid partition coefficients. The nonmetals, S, P, and C, which are largely excluded from the crystallizing Fe-Ni so they become enriched in the residual melts, can drastically modify the partition coefficients of the metallic elements. Iron meteorites mostly contain 0.02–2 wt.% S in the form of troilite (FeS), although S is relatively insoluble in solid Fe-Ni (*Buchwald,* 1975). Troilite nodules in irons, which may have diameters of a centimeter or more, probably formed from melt that was trapped during crystallization. Fractional crystallization modeling suggests that group IVB irons crystallized from a melt that contained <1 wt.% S as the linear trends on log-log interelement plots can be modeled with fixed partition coefficients (*Chabot,* 2004). However, groups IIAB, IID, IIIAB, IVA appear to have crystallized from magmas with ~5–20 wt.% S and typically show nonlinear trends on log-log plots. The near absence of such S-rich irons is attributed to the low strength of troilite relative to Fe-Ni. Many iron meteoroids survived in space for hundreds of million years as meter-sized objects. Their cosmic-ray exposure ages are roughly 10× longer than nearly all stony meteorites (*Herzog and Caffee,* 2014).

4.2.1. Formation of fractionally crystallized groups. Three large groups of iron meteorites, IVA, IIIAB, and IVB, have chemical properties consistent with formation in a large metallic core, but other properties indicating they did not cool in a core surrounded by a silicate mantle. For the IVA irons, there are three pieces of evidence. First, their metallographic cooling rates at ~500°C vary from 100° to 6000°C m.y.$^{-1}$, whereas samples from a well-insulated metallic core should have essentially uniform cooling rates at ~1200°C. Second, the ancient Pb-Pb age of troilite in one IVA iron of 4564 Ma (*Blichert-Toft et al.,* 2010) (Fig. 1) is far too old for a core sample from a large asteroid, which would take ~100 m.y. or more to cool. Third, two IVA irons contain abundant silicates with anomalously rapid cooling rates (*Haack et al.,* 1996; *Ruzicka,* 2014). Although the nonuniform metallographic cooling rates in IVA have been questioned (*Wasson and Hoppe,* 2012), several features support

a wide range of cooling rates among the IVA irons. These include the dimensions of the submicrometer intergrowth called, "cloudy taenite," and the composition of the kamacite and taenite and their interface (*Goldstein et al.,* 2014).

The thermal history and age of group IVA irons can be explained if the original IVA asteroid was disrupted after melting to form a metallic body with a radius of 150 ± 50 km surrounded by <1 km of silicate mantle (*Yang et al.,* 2007, 2008). Thermal and fractional crystallization modeling shows a good match between calculated and observed cooling rates for a body that crystallized radially inward (Fig. 5). Separation of core from silicate mantle was probably caused by hit-and-run impacts as conventional hypervelocity impacts are very inefficient at separating core and mantle material (*Asphaug et al.,* 2006; *Asphaug and Reufer,* 2014) (see section 5).

Group IIIAB, which is the largest group of iron meteorites with over 200 members, has a cooling rate range of 60°–300°C m.y.$^{-1}$ and phosphates that cooled through ~750°C about 4 m.y. after CAI formation (*Sugiura and Hoshino,* 2003; *Yang and Goldstein,* 2006) (Fig. 1). These constraints can be accommodated by a metallic body with a radius of several tens of kilometers that cooled with only a few kilometers of silicate mantle (*Goldstein et al.,* 2009). Cosmic-ray exposure ages of IIIAB and IVA irons cluster around 650 and 400 Ma, respectively (*Herzog and Caffee,* 2014). These ages were previously interpreted as the breakup events for the entire IIIAB and IVA metallic cores (*Keil et al.,* 1994), but it is possible that they date the destruction of relatively small but representative rubble piles of metal fragments (*Yang et al.,* 2008).

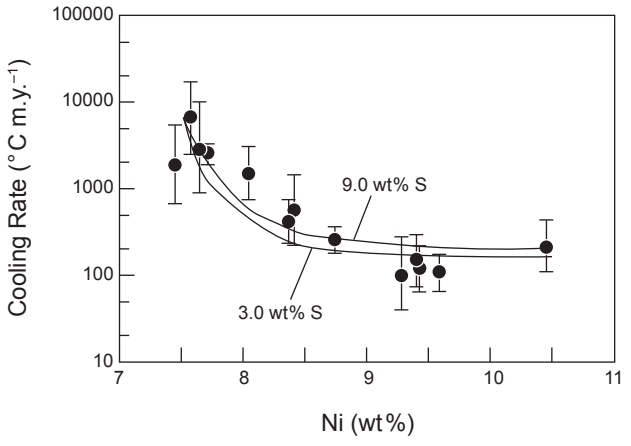

Fig. 5. Metallographic cooling rates at 500°C for 13 group IVA irons decrease with increasing bulk Ni. The curves show calculated cooling rates for a metallic body of radius 150 km that lacks a silicate mantle. The depth of each iron in the metallic body is inferred from its Ni concentration and fractional crystallization modeling assuming bulk S contents of 3 or 9 wt.%. The original IVA parent body, which would have had a minimum radius of 300 ± 100 km, is thought to have been disrupted by a hit-and-run collision ~2 m.y. after CAI formation. After *Yang et al.* (2008).

Group IVB irons cooled through 600°–400°C at rates of 500°–5000°C m.y.$^{-1}$ that increase with increasing bulk Ni (*Yang et al.,* 2010b). They appear to be derived from a metallic body that crystallized outward and was 65 ± 15 km in radius when cooling without a silicate mantle. Separation of the mantle from a solid core may have occurred after the core was largely solid and could have been aided by a thin layer of residual metallic melt between core and mantle. In this case, the IVB irons may have crystallized in a mantled core that was somewhat larger (70 ± 15 km in radius). Group IVB irons are unrelated to any other meteorite type (*Krot et al.,* 2014).

4.2.2. Formation of silicate-rich irons. Iron meteorites in groups IAB, IIE, and IIICD, which have very different chemical trends from the fractionally crystallized groups, contain numerous silicate inclusions. Textural and mineralogical evidence suggests they formed by impact-mixing of previously heated silicate and molten metal (*Ruzicka,* 2014). Group IAB irons contain angular fragments of chondritic material, except for Caddo County and Ocotillo, which contain highly differentiated silicates. The chemical and oxygen isotopic composition of the silicates in IAB and IIICD irons closely match those of silicates in winonaites, which are strongly metamorphosed and partly melted chondrites (Table 2), suggesting they come from the same asteroid. The low degree of silicate melting of winonaites and most silicate inclusions in IAB irons suggests that temperatures were not high enough to allow a metallic core to form in their parent body (*Benedix et al.,* 2014). The time of impact mixing of metal and silicate was inferred by *Vogel and Renne* (2008) from Ar-Ar ages to be ~4480 Ma, but Hf-W and Pd-Ag isotopic systematics favor several impacts ~2–10 m.y. after CAI formation (*Schulz et al.,* 2012; *Theis et al.,* 2013). Low shock levels in the IAB silicates and winonaites suggest that low-speed accretionary impacts mixed metal and silicate, although impacts at the current mean asteroidal impact speed of ~5 km s^{-1} are not efficient at creating shocked and melted rock (*Marchi et al.,* 2013) and cannot be excluded.

Group IIE irons have relatively uniform Fe-Ni compositions and diverse silicate inclusions that range from chondritic in composition and texture to highly differentiated basaltic and glassy inclusions. The oxygen isotopic composition and the mineralogy of the chondritic inclusions resemble those of H chondrites, although the IIE silicates appear to be slightly more reduced. They were probably formed by impacts onto an H-like chondritic body, which experienced significantly more melting than the IAB-winonaite body (Ruzicka, 2014). Since most of the IIE irons have highly differentiated silicates, it is possible that the IIE metal was derived from a molten metal core in a body with a chondritic crust (*Weiss and Elkins-Tanton,* 2013; see also the chapter by Scheinberg et al. in this volume). The impact that mixed metal and silicate occurred at ~4.5 Ga. During the late heavy bombardment at ~4 Ga, the IIE body was presumably still very large as many IIE irons have strongly shocked silicate inclusions with Ar-Ar ages of 3.7–4.0 Ga (*Bogard,* 2011) (see section 4.4.1).

4.3. Stony-Iron Meteorites

Two major types of stony-irons — pallasites and mesosiderites — are known (Table 2). Both appear to have formed in impacts that mixed largely unshocked silicate and molten metallic Fe-Ni (*Benedix et al.,* 2014; *Krot et al.,* 2014). Pallasites, which formed by impact mixing of core metal with mantle olivine, are largely from the so-called "main group." Five Eagle Station types constitute a second group and there are another ~5–7 ungrouped pallasites.

Diverse cooling rates and paleomagnetic properties show that the main-group pallasites did not cool at the core-mantle boundary of an asteroid (*Yang et al.,* 2010a; *Tarduno et al.,* 2012). Metal and possibly some olivine were probably extracted by a low-velocity impact with a larger body (*Asphaug et al.,* 2006) and deposited in the mantle of the larger body that contained a core-dynamo. Interestingly, there are no iron or olivine-rich meteorites that are genetically related to the main-group or Eagle Station pallasites. [IIIAB irons were once thought to be related to the main group, but their cooling rates and chemical compositions suggest they crystallized inward, whereas the metal in main-group pallasites was probably derived from a core that crystallized outward (*Yang et al.,* 2010a)]. Metal was efficiently mixed with olivine so that olivine-free metal regions are ≤1 m in size, and olivine mantle chunks without metallic armor were fractured along grain boundaries and are too weak to survive as meteorites. The time of metal-olivine mixing is not well constrained, but Mn-Cr systematics suggest 4558 Ma or possibly earlier for the main group (*Lugmair and Shukolyukov,* 1998).

Mesosiderites formed by mixing of basaltic and gabbroic silicate from a Vesta-like body with molten Fe-Ni, probably from the core of a second asteroid (*Benedix et al.,* 2014). They cooled through 500°C slower than any other meteorites at ~0.5°C m.y.$^{-1}$ for ~700 m.y. (*Goldstein et al.,* 2014). Argon-argon ages of 3.7–4.0 Ga reflect slow cooling, not impact reheating or excavation (*Bogard,* 2011). The anomalous mesosiderite Chaunskij contains cordierite, which formed at a pressure of 6 Kbar, probably in a body that was >400 km in radius (*Petaev et al.,* 2000). The time of metal-silicate mixing was previously thought from Sm-Nd ages of clasts to have been ~100–150 m.y. after CAIs (*Stewart et al.,* 1994), but a reinterpretation of these ages by *Ganguly and Tirone* (2001) suggests that they date slow cooling and that molten metal and silicate were mixed at 4.56 Ga. The low shock levels in pallasites and mesosiderites and the efficient mixing of molten metal with silicate suggest that mixing occurred during accretion in a low-velocity impact.

4.4. Achondrites

4.4.1. Eucrites. The largest group of achondrites — the howardites, eucrites, and howardites, which are eucrite-diogenite breccias — are almost certainly from (4) Vesta (*McCord et al.,* 1970; *Keil,* 2002; see also the chapter by Russell et al. in this volume). Vesta is a unique body as it appears to be the only differentiated asteroid that has retained its core, mantle, and basaltic crust. [For a contrary view, see *Consolmagno et al.* (2015).] Although the effects of early impacts are commonly neglected, impacts were common during igneous processing, as many diogenites and eucrites have excessively high concentrations of siderophiles. *Dale et al.* (2012) attribute these high siderophile concentrations and those in other achondrites to chondritic projectiles. However, differentiated projectiles with molten cores and mantles cannot be excluded, as they also have chondritic bulk compositions.

Most eucrites and diogenites were strongly shocked and brecciated at 3.7–4.1 Ga during the late heavy bombardment (*Bogard,* 2011; *Marchi et al.* 2013), but a small group of pristine unshocked eucrites with Ar-Ar ages of 4.48 Ga may have been removed from Vesta long before the other eucrites. (This Ar-Ar age should be increased by ~0.03 Ga to allow for half-life and other corrections.) *Bogard and Garrison* (2003) suggested that they were extracted from Vesta by a hypervelocity impact at that time and stored in a small body. Small asteroids that survived the late heavy bombardment intact lack shock-heated meteorites from this era. Large asteroids preferentially retain shocked rocks more efficiently and sustain larger, high-velocity impacts that deposit vastly more impact energy per kilogram of target (see also *Marchi et al.,* 2013).

At least two ungrouped eucrites, NWA 011 and Ibitira, and possibly several others, are isotopically and chemically so different from normal eucrites that they probably come from other bodies (*Mittlefehldt,* 2005; *Scott et al.,* 2009; *Sanborn and Yin,* 2014). These bodies were probably >100 km in radius, as smaller bodies would probably have lost their basalts during explosive volcanism (*Wilson and Keil,* 1991). The ungrouped eucrites, unlike normal eucrites, appear to have escaped the effects of the late heavy bombardment and may have been extracted from their parent bodies before 4.0 Ga, like the 4.48-Ga-old unbrecciated eucrites. The ungrouped eucrites are not related to other types of achondrites or iron meteorites and are plausibly fragments from the small V-type asteroids that orbit far beyond Vesta (section 3.1).

4.4.2. Angrites. Angrites are unbrecciated and substantially unshocked igneous rocks of roughly basaltic composition that have preserved a record of early igneous activity in a large asteroid and paleomagnetic evidence for a core dynamo (*Weiss et al.,* 2008; *Keil,* 2011). Hafnium-tungsten isotopic data show that the core formed <2 m.y. after CAIs but not in a single event from a homogeneous magna ocean. *Kleine et al.* (2012) infer that planetesimals impacted the angrite parent body during core formation. The lack of shock and breccia features in angrites suggests they were removed from their parent asteroid before the late heavy bombardment (*Scott and Bottke,* 2011), like the unbrecciated eucrites (*Bogard and Garrison,* 2003).

4.4.3. Aubrites. Aubrites, which are enstatite achondrites, are regolith or fragmental breccias and are probably derived from one or more E-type asteroids in the Hungaria region (section 3.4). The absence of associated metal-rich meteorites or asteroids suggests that these asteroids may

have been emplaced in the Hungaria region after disruption of their parent asteroid. One ungrouped aubrite, Shallowater, which contains about ~15% of inclusions of enstatite chondrite material, provided the first meteorite evidence for very early major impacts that involved a molten planetesimal. *Keil et al.* (1989) inferred that Shallowater formed after a chondritic projectile had disrupted a molten aubritic body during a low-velocity impact. The chondritic material may also have been derived from an unmelted crust on the molten body. The ancient I-Xe age of Shallowater of 4561 Ma (Fig. 1) shows that this impact occurred about 5 m.y. after CAI formation. The thermal history of the metal grains suggests that the parent asteroid suffered two other catastrophic impacts as it cooled (*Keil et al.,* 1989).

4.4.4. Ureilites. Ureilites are coarse-grained carbon-bearing ultramafic rocks that formed as residues from partial melting at temperatures of ~1100°C (*Krot et al.,* 2014). The presence of uninverted pigeonite, or nanometer-scale augite exsolution lamellae (*Mikouchi et al.,* 2010), and high-Ca olivine shows that ureilites rapidly cooled from ~1100°C to <650°C in hours, and the high level of shock effects in silicates suggests that this resulted from a hypervelocity catastrophic impact (*Goodrich et al.,* 2004, 2015). To cool in hours, the fragments must have been meter-sized prior to reaccretion. The energy for dispersing the fragments was not solely kinetic as the effect of the impact was analogous to removing the cork from a champagne bottle. The reduction in lithostatic pressure allowed carbon to react with silicates, forming a CO-CO_2 mixture and leaving tiny Fe metal grains on the edges of the olivine grains. Release of gas helped to catastrophically fragment the rock and temporarily disperse the fragments. The impact probably occurred 5 m.y. after CAIs (Fig. 1), as this is the age of basaltic fragments from ureilite breccias containing feldspar crystals and glass (*Goodrich et al.,* 2010, 2015).

4.5. Primitive Achondrites

Several groups of meteorites experienced low degrees of melting and mobilization of silicate and FeNi-FeS phases. They are commonly called primitive achondrites and include acapulcoites, lodranites, brachinites, and winonaites (Table 2) (*Krot et al.,* 2014). The least-metamorphosed acapulcoites and winonaites still contain rare relict chondrules but most primitive achondrites have recrystallized, granular textures and are typically enriched or depleted in low-temperature silicate and metallic melts. None of these meteorites are fragmental breccias and most are unshocked or only lightly shocked (stages S1–S2). Note that there are no clear-cut divisions between achondrites and primitive achondrites. Brachinites, for example, are considered by some authors to be achondrites, and ureilites have also been classed as primitive achondrites.

4.5.1. Acapulcoites and lodranites. Acapulcoites have near-chondritic chemical compositions whereas lodranites were heated to higher temperatures and are commonly richer in metal. They clearly formed in close proximity, as some meteorites contain both types of material due to mixing and rewelding of hot material, and others have intermediate characteristics. These meteorites have two unusual characteristics. First, metallographic cooling rates of seven acapulcoites and lodranites are 10^3–10^4°C m.y.$^{-1}$ (*McCoy et al.,* 1996, 1997) — one or more orders of magnitude higher than maximum rates for material in undisturbed asteroids heated by ^{26}Al (*Scott et al.,* 2014). Second, Ar-Ar ages of seven of these meteorites are remarkably similar: 4512 ± 9 Ma (*Bogard,* 2011). Since their diverse textures require different formation locations, their common age and rapid cooling rate suggests they were all extracted from depth by an impact, possibly a catastrophic one, before their parent body had cooled significantly. Given the well-determined Pb-Pb age of Acapulco phosphate of 4556 ± 0.5 Ma (*Göpel and Manhes,* 2010), and the required increase in the Ar-Ar ages by 30–40 m.y. due to errors in the ^{40}K decay rate (*Bogard,* 2011), it is likely that this large impact occurred 11 m.y. after CAI formation. Thermal models that assume that cooling was undisturbed by impacts (e.g., *Golabek et al.,* 2014) can only provide very approximate constraints on parent-body size and burial depth.

4.5.2. Brachinites. Brachinites are ancient unbrecciated and essentially unshocked rocks that are largely composed of FeO-rich olivine and pyroxene (Table 2) with heterogenous Δ^{17}O values consistent with low degrees of melting (*Greenwood et al.,* 2012; *Keil,* 2014). There are no firm constraints on their cooling rates, but CaO concentrations in olivine are 0.08–0.3 wt.%, higher than in acapulcoite-lodranites but not as high as in ureilites (*Krot et al.,* 2014). Thus brachinites cooled rapidly enough to prevent Ca diffusing out of olivine suggesting that, like ureilites and acapulco-lodranites, they were excavated from depth by impact before they had cooled below ~1000°C.

4.6. Differentiated Meteorite Parent Bodies

There are few genetic relationships among differentiated meteorites apart from the link between winonaites and IAB irons, which are probably not derived from core metal. We lack mantle or crust material from the 60-odd parent bodies of the grouped and ungrouped iron meteorites and we lack core material from the parent bodies of the various groups of achondrites and the numerous ungrouped achondrites, such as the ungrouped eucrites, Graves Nunataks (GRA) 06128 and Divnoe, which are listed in the Meteoritical Bulletin Database (see *http://www.lpi.usra.edu/meteor/metbull.php*). Our collection of differentiated meteorites resembles a collection of 1000 pieces from ~100 different jigsaw puzzles with 1–100 pieces from each puzzle. Notably missing are the olivine-rich mantle meteorites from the parent bodies of irons, stony-irons, and achondrites.

Early impacts during the first few million years are needed to remove mantles from core material or mix molten metal and silicate and to explain the properties of IIIAB, IVA, and IVB irons, pallasites, mesosiderites, and the Shallowater aubrite. Disruption of the ureilite body and

formation of CB chondrules require later hypervelocity impacts ~5 m.y. after CAI. The IAB irons, acapulcoites and lodranites, brachinites, angrites, and anomalous eucrites were involved in major early impacts that left little evidence for shock consistent with accretionary impacts. However, some of these impacts could have occurred after asteroid accretion given that typical asteroidal impacts at current impact speeds of ~5 km s^{-1} create relatively little shocked material (*Marchi et al.,* 2013).

Interestingly, the metal-bearing meteorites that cooled slowest at ~500°C are the IAB irons, the pallasites, and the mesosiderites. In each case, cooling rates are rather uniform although the meteorites are not from asteroidal cores. Iron meteorites that are probably derived originally from core material, like IIIAB, IVA, and IVB irons, cooled faster than the stony-irons and silicate-rich IAB irons, and each group shows a wide range of cooling rates. This is the exact opposite of what conventional models predict. If the core samples had cooled *in situ*, their cooling rates would be uniform in each group and generally slower than those that cooled in smaller metallic pools. These cooling rates may be understood, however, if differentiated bodies were torn apart during accretion by hit-and-run collisions when the cores were still molten or partly molten (*Asphaug et al.,* 2006). Below, we review how these impacts differ from conventional hypervelocity impacts in the current asteroid belt and how they might explain the meteoritic evidence for early low-speed impacts between planetesimals.

5. HIT-AND-RUN COLLISIONS

Conventional hypervelocity impacts are not effective at excavating core material from differentiated asteroids and liberating iron meteoroids as they require exceptionally large projectiles having half the target's size and, in the case of Vesta-sized bodies, exceptionally fast impact speeds (*Asphaug,* 2010). By contrast, grazing impacts during early planet formation at velocities comparable to the escape velocities of the colliding bodies are remarkably effective at disrupting differentiated bodies (*Agnor and Asphaug,* 2004; *Asphaug et al.,* 2006; *Stewart and Leinhardt,* 2012). These collisions result in a very odd assortment of relics by introducing a mechanism for winnowing or stripping the lower-density mantle, crustal, and hydrospheric components from the denser deep mantle and iron core components, forming bodies whose compositions can depart substantially from the chondritic average (*Asphaug and Reufer,* 2014).

5.1. Self-Stirred Populations

Although we do not yet know how planetesimals formed, the modern assumption is that there was a phase of rapid growth that formed bodies 100 km in diameter or larger (*Weidenschilling and Cuzzi,* 2006; see also the chapter by Johansen et al. in this volume). This means that a population of similar-sized protoplanets or planetary embryos was accreting early on. Similar-sized collisions ($R_1 \sim R_2$) are remarkably different from cratering impacts, there being no locus to the collision. Due to geometrical effects, most of them are grazing events where the colliding matter continues downrange (*Asphaug,* 2010).

According to classic theories (*Safronov,* 1972; *Wetherill,* 1980), in the absence of damping by nebula gas such a population becomes gravitationally stirred by close mutual encounters, to random relative velocities v_{rel} comparable to the escape velocity v_{esc} of the largest bodies. The impact velocity $v_{imp} = \sqrt{(v_{rel}^2 + v_{esc}^2)}$ where $v_{esc} = \sqrt{2G(M_1+M_2)/(R_1+R_2)}$ is the escape velocity, the speed at which two spherical planets of masses $M_1 > M_2$ and radii R_1 and R_2 collide if falling from "infinity" with zero relative velocity. It is about equal, in meters per second, to the diameters of the colliding bodies, in kilometers, thus around 100 m s^{-1} during planetesimal accretion and around 10 km s^{-1} during late-stage planet formation. Impacts occurring during planetesimal accretion would not generally have involved shocks.

Relative motions are damped by smaller planetesimals and gas, and are excited by larger embryos and by resonant gravitational perturbations by large planets outside the protoplanetary region. There is always some random relative velocity, so that impacts are always somewhat faster than v_{esc}. Accretion is never completely efficient, but the surprising thing is that only a modest random velocity, $\sim(2/3)v_{esc}$, is sufficient to reduce accretion efficiency so that hit-and-run collisions are as frequent as coagulation (*Agnor and Asphaug,* 2004; *Asphaug,* 2010). Moreover, it makes the disruption behave in a systematically biased sort of way, as we shall see.

Disruption in turn feeds back into the population of small particles that can damp velocities, so that accretion efficiency can go back and forth as early planet formation continues. Meteorites that constitute the record of this epoch are therefore expected to represent this wide range of outcomes: effective coagulation, and more energetic mantle-stripping impacts. The outcomes that do not ultimately result in accretion into planets are those that are sampled by the meteorite collection.

The accretion efficiency ξ is defined as $(M_F - M_1)/M_2$ where $M_F < M_1 + M_2$ is the mass of the final largest body (*Asphaug,* 2009). For velocities characteristic of late-stage planet formation, $0.7 \le v_{rel}/v_{esc} \le 2.5$, it has been shown that about half of similar-sized collisions are hit and run ($\xi \approx 0$), in which M_2 bounces off or plows through M_1, becoming a mantle-stripped relic or chain of iron-rich bodies (*Agnor and Asphaug,* 2004; *Asphaug et al.,* 2006; *O'Brien et al.,* 2006; *Asphaug,* 2009; *Chambers,* 2013).

Higher-velocity collisions with $v_{rel}/v_{esc} \ge \sim 3$ erode increasing fractions of the target ($\xi < 0$). But catastrophic disruption of M_1 requires $v_{imp} \gg v_{esc}$, so does not occur during accretion. Catastrophic disruption of M_2, on the other hand, is an intimate aspect of pairwise accretion, even under low relative velocities. The sensitivity of ξ over the expected velocity range leads to spectacularly diverse non-accretionary outcomes, and to the evolution, by attrition, of a highly varied assortment of unaccreted objects — mantles segregated from cores by hit-and-run events and partial accretions.

5.2. Mantle Stripping During Accretion

Mantle stripping during accretion has little to do with blasting material from the target into orbit or into escaping trajectories. This is especially the case for planetesimal accretion, where the collisional velocities are too slow to induce shocks. Rather, it is the two-body interaction that causes mantle material to be lost. It is not blasted off the target; it is unaccreted from the projectile.

Lower-density materials at or near the surface of M_2 (i.e., the mantle, crust, hydrosphere, and atmosphere) are slung onto noncapture trajectories, while higher-density materials can be stopped effectively and sink to join the target core, or can skip off the target and be segregated into chains of iron-rich clumps and iron-poor debris. Before we present simulations of examples of such events, here we simply notice two facts: (1) the diversity of outcomes is enormous, and (2) to first order, hit and run is as common as accretion.

One very important dynamical fact is that mantle stripping by hit and run provides a permanent sink for these "lost" (unaccreted) silicates that are missing from our meteorite collections. Following a hit-and-run collision, the target M_1 is orbiting the Sun along with M_2 on crossing orbits. The collisional cross section of M_1 is larger than M_2 by approximately the geometric cross section $\sim R_2 \times$ the gravitational focusing $f = 1 + (v_{esc}/v_{rel})^2$, the latter increasing with $R \propto v_{esc}$. Consequently M_1 accretes most of the stripped mantle from M_2 during the thousands of orbits following a collision.

While M_1 sweeps up most of the debris, it will likewise sweep up M_2 in one or more subsequent collisions, causing M_2 to disappear unless gravitational perturbations or tidal migrations or other collisions isolate it from M_1. This has sometimes been regarded by dynamical modelers as discounting the relevance of hit-and-run collisions, since eventually all the mess gets swept up by M_1.

But when one considers the statistics of survivors — i.e., the attrition bias of the relics of planet formation (*Asphaug and Reufer,* 2014) — one finds that in fact survivors of multiple hit-and-run collisions will not only be present, but will be common in typical pairwise-accretion scenarios. If a population of N bodies accretes forming planets and leaves behind N_{final} unaccreted original bodies, then the average number of hit-and-run collisions experienced by the unaccreted remnants will be approximately $h \sim \ln(N/N_{final})$. The stronger the attrition (the smaller N_{final}/N), not only the greater the average h, but the wider the spread in h — i.e., the greater the diversity.

On this basis, *Asphaug and Reufer* (2014) argue that Mars and Mercury, if original remnants of an original ~20 bodies that accreted to form Earth and Venus, would be expected to have one survivor of ~2 hit-and-run collisions, and one survivor that is relatively unperturbed by unaccretionary collisions. If tens of thousands of planetesimals accreted to form a few thousand asteroid progenitors, then h = ~3. Bodies like (16) Psyche and the stripped cores of the iron meteorite parent bodies could have experienced several hit-and-run collisions as the accretionary mergers took place, while Vesta would be a survivor of few if any hit-and-run collisions.

While it may seem far-fetched to invoke multiple hit-and-run collisions for mantle stripping of planetesimals and planetary embryos, the theoretical basis for this idea has been established, and is in fact validated to some extent in the latest dynamical models. In the first N-body integrations to track the remnants of hit-and-run collisions, *Chambers* (2013) finds cases where terrestrial protoplanets experience multiple hit-and-run collisions and then become dynamically isolated. Obviously there is much work to be done on understanding the influence of imperfect accretion on the dynamics of planet formation; here we now look more closely at the aftermath of such encounters between planetesimals.

5.3. Subsonic Hit-and-Run

Subsonic hit-and-run collisions between planetesimals are as effective at removing mantle silicates as their hypervelocity counterparts between embryos, but do so differently as illustrated by comparison simulations (Fig. 6), where $M_2/M_1 = 0.20$, $\theta = 30°$, $v_{imp} = 3\ v_{esc}$, but one is subsonic, the other supersonic. In each case the core and mantle are effectively segregated, but the collision on the right, into an Earth-mass target, induces strong shocks that vaporize the escaping material and cause its dispersal. The smaller collision on the left, into a target 0.01 $M_\oplus$ but otherwise similar in scale, shreds M_2 according to subsonic mechanical and gravitational interactions, segregating it by density into chains of metal-rich and metal-free clumps, without shock heating.

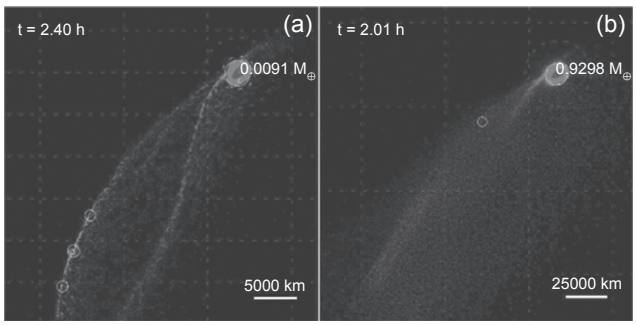

Fig. 6. See Plate 19 for color version. Simulations of two collisions with the same $M_2/M_1 = 0.2$, $\theta = 30°$, $v_{imp} = 3\ v_{esc}$, but differing in mass by a factor of 100. Both are shown at ~10 collision times, $\tau_{coll} = 2(R_1 + R_2)/v_{imp}$. Silicates (red) are segregated from metals (blue) in the remnants of M_2 and are dispersed downrange in both hit-and-run collisions. The subsonic collision (left; $R_1 = 1400$ km, $R_2 = 800$ km) leads to a chain of iron-dominated clumps (white circles) stripped gravitationally and mechanically from a sheet of lower-density mantle material. The supersonic collision (right; $M_1 = M_\oplus$, $v_{imp} \approx 30$ km s^{-1}), produces intense global shocks and fine dispersal of the plume. After *Asphaug and Reufer* (2014).

Subsonic hit-and-run collisions among accreting planetesimals provide an evolutionary pathway that is perhaps highly relevant to the major asteroids such as Psyche that appear metallic and the parent asteroids of iron meteorites that also lost their mantles (*Yang et al.,* 2007; *Goldstein et al.,* 2009) (section 4.2.1). Removal of mantles from cores by conventional hypervelocity impacts (e.g., *Burbine et al.,* 1996) is a long-standing problem, as it requires repeated giant impacts from projectiles with half the target's size, while leaving Vesta's crust intact (*Davis et al.,* 1985).

Iron fraction and diversity in this scenario are not an aspect of the planetesimals' starting compositions — they all might start out chondritic — but a consequence of varying the number and type of hit-and-run collisions experienced by each survivor. It is unlikely for an asteroid parent body to have suffered repeated hit-and-run collisions during terrestrial planet formation, but it is even less likely for it to have not been accreted. This motivates the attrition bias argument (*Asphaug and Reufer,* 2014) for the preponderance of hit-and-run relics among asteroids. To not be accreted means to either be dynamically isolated from the accretionary swarm from the beginning (h = 0), or to be lucky (unaccreted; hit and run) every time there is a collision with a larger body. So in the end, this selection bias strongly influences the surviving population.

The timing of all these collisions would have been very early, within the first few million years when the planetesimals were growing into protoplanetary embryos. Multiple mantle-stripping impacts while the bodies were solidifying would be the right recipe for a thin-skinned solidifying core such as is inferred from modeling of the IVA iron cooling rates (section 4.2.1). However, detailed modeling is needed that feeds the output of the first hit-and-run collision, into a second hit-and-run collision, and a third.

Of course, as Fig. 6 makes clear, not all the hit-and-run remnants are iron-rich clumps. Some hit-and-run collisions swallow the core and leave the mantle escaping downrange (*Reufer et al.,* 2012). Such impacts could account for the formation of stony-irons (section 4.3). Subsonic hit-and-run collisions leave behind surviving blobs of silicate relics subject to varying degrees of deformation and pressure release (*Asphaug et al.,* 2006), whose genetic relationship to irons would be complex — a topic of further study.

6. COLLISION AND DYNAMICAL EVOLUTION MODELS

If differentiated asteroids were derived from numerous Vesta-like bodies as a result of impacts in the asteroid belt, the distribution of differentiated asteroids would be very different from what we observe today. Collision and dynamical evolution modeling indicates the asteroid belt has experienced a limited amount of collisional evolution over its history (see the chapter by Bottke et al. in this volume). The existence of a very small number of differentiated asteroid families in the current main belt, the survival of Vesta's crust, and the fact that Vesta only has two very large basins collectively suggest that comminution in the asteroid belt has been insufficient to disrupt numerous differentiated bodies down to their cores and erase silicate fragments. It appears likely that only a modest number of large fully and partially differentiated bodies ever existed in the main belt, and most of these (like Vesta) were large enough to survive intact to recent times.

To test this assertion, we have explored a scenario where Vesta once had "sister" objects in the main belt (*Bottke,* 2014). The idea would be that the asteroid belt once had considerably more mass in its primordial era, including several Vestas, but that most of this material was eliminated by a dynamical depletion process, such as sweeping resonances associated with planet migration, ejection of material by interaction with planetary embryos, or Jupiter migrating across the asteroid belt in the Grand Tack model (*Walsh et al.,* 2011, 2012; see also the chapter by Morbidelli et al. in this volume). This would potentially allow ancient cratering events on Vesta's long-lost sisters to explain the V-types seen in the central and outer main belt.

Our simulations used *Boulder*, a collisional code capable of simulating the dynamical depletion and collisional fragmentation of multiple planetesimal populations using a statistical particle-in-the-box approach (*Morbidelli et al.,* 2009**).** We input into *Boulder* an estimate of the primordial main-belt size distribution stretched across many semimajor axis zones as well as a preset number of Vesta-like objects. The primordial main belt was assumed to be N times larger than the currently observed population and simulations were run with 1, 2, 3, . . ., N Vestas in that population. We tracked these populations and their fragments for hundreds of millions of years until the putative time of late giant planet migration at ~4 Ga. At that time, we assumed that a dynamical depletion event took place that removed most of the main belt's excess mass. From that point, collisional grinding over the next 4 G.y. was set to reproduce the current main-belt population. Over all this, we assumed that impacts on Vesta-like objects would produce fragments that were distinct (in spectroscopic signatures, colors, and albedos) from background asteroids, as the V-types are today in the main belt. When the model reached the current time, a successful run was one that was able to reproduce the current main belt and the observed V-type size distributions in the inner and central/outer main belt within tolerance limits.

Our results, while still preliminary, suggest the history of Vesta and her putative sisters can be used to constrain main-belt history. We find that an excited primordial main belt with more than 3–4 Vestas after the first few million years of its history produces too many V-type fragments compared to observations; collisonal and dynamical evolution over 4.5 G.y. cannot get rid of all the evidence. Accordingly, it is likely that *fewer* than 3–4 Vestas existed in the main-belt region after the first few million years of its history. Collisions on these bodies prior to their dynamical removal are a plausible way to explain the V-types seen in the central/outer main belt, provided dynamical mechanisms allow one to get rid of Vesta's sisters at a later time. These results are also consistent with dynamical work indicating that the

primordial asteroid belt only lost, at best, a factor of ~1–4× its population during giant planet migration as described by the Nice model (see the chapter by Morbidelli et al. in this volume). Perhaps more importantly, this scenario shows how difficult it is for collisional evolution in the main belt to produce the putative core and mantle fragments observed today; if impacts could easily extract this material from the depths of differentiated asteroids like Vesta, one would also expect to see many more V-type and related asteroids.

6.1. Differentiated Planetesimals and Their Fragments from the Terrestrial Planet Region

To glean insights into the origin of the differentiated material in the asteroid belt, it is useful to take a step back and consider this issue from the perspective of planetesimal formation, namely accretion timescales and planetesimal heating mechanisms.

While precise accretion timescales for planetesimals forming all across the inner solar system are unknown (see the chapter by Johansen et al. in this volume), modeling work suggests they probably vary with swarm density and semimajor axis, such that accretion timescales become longer with increasing heliocentric distance, at least until the so-called "snowline" is reached. Given that ^{26}Al was the major heat source for melting asteroids (section 2.2), the earliest planetesimals would have formed in the terrestrial planet region and they are more likely to be heavily metamorphosed or differentiated compared to same-sized bodies forming in the asteroid belt. Interestingly, this internal heating trend is largely consistent with trends observed among large main-belt asteroids: S-complex asteroids, believed to be analogous to metamorphosed but unmelted ordinary chondrites, dominate the inner main belt, while C-complex asteroids, many analogous to more primitive carbonaceous chondrites, dominate the outer main belt (see the chapter by DeMeo et al. in this volume).

The best place to form large differentiated planetesimals may also be the most likely location for them to undergo hit-and-run collisions. In the first few million years of solar system history, the terrestrial planet region was filled with planetary embryos and differentiated planetesimals (see the chapter by Morbidelli et al. in this volume). Collisions between these bodies would have been common, with the outcome leading to terrestrial planets. Hit-and-run collisions between differentiated planetesimals and larger protoplanets in the interim would have led to numerous aggregates made up of diverse proportions of crust, mantle, and core, as well as a sea of smaller fragments. These bodies would then undergo their own collisional and dynamical evolution, with the vast majority lost by comminution, by accretion with larger bodies in the terrestrial planet region, or by being ejected out of the inner solar system via a Jupiter encounter. Only the largest, strongest, or most fortunate bodies would survive for very long. We speculate that the population of objects left behind by hit-and-run collisions includes the M-type asteroids, some which are exposed core material, and others of which may be a "hodgepodge" of crust, mantle, and core (referred to here as hodgepodge worlds). In addition, these collisions would have generated A-type asteroids and possibly some S-types that are also hodgepodge bodies. (We infer that V-types have deep spectral features with little space weathering because they lack metal and troilite, and that metal/troilite mixed with differentiated material will be space weathered so that it has spectral properties like S-type asteroids.)

Bottke et al. (2006) argued on these grounds that some fraction of the differentiated planetesimals made their way into the main belt region via early dynamical processes. Subsequent evidence for the early destruction of molten or semimolten parent bodies of iron meteorites (section 4.2) suggests that the flux of material from the terrestrial planet region into the asteroid belt may have been dominated by debris from differentiated planetesimals. This process helps to explain why the asteroid belt has a larger-than-expected number of fragments that appear to come from differentiated planetesimals, yet could still be dominated by nondifferentiated material. The wide variety of parent bodies represented in iron meteorites would also be naturally explained as a byproduct of collisional and dynamical evolution of planetesimals and protoplanets in the terrestrial planet region. We infer that the parent bodies of non-Vestan differentiated meteorites were largely disrupted before they were inserted into the asteroid belt, rather than "battered to bits" *in situ* within the asteroid belt (*Burbine et al.,* 1996).

6.2. Dynamical Scenarios for Captured Assemblages of Differentiated Materials

Here we present several dynamical scenarios that could plausibly move material from the terrestrial planet zone to stable orbits within the main-belt region.

The first, and arguably the simplest, involves gravitational scattering among planetary embryos (*Bottke et al.,* 2006). Here planetesimals and their fragments evolved amid a swarm of Moon- to Mars-sized bodies spread between Mercury's current location to within the asteroid belt. In this scenario, the S- and C-complex asteroid populations that dominate the various zones of the asteroid belt (e.g., *Petit et al.,* 2002; *DeMeo and Carry,* 2014) were assumed to form more or less *in situ*, such that only a rather limited amount of material was scattered outward from the terrestrial planet region into the asteroid belt.

Numerical runs show that even a few million years is sufficient to scatter a small fraction of terrestrial planet material onto stable orbits within the main-belt zone, provided the planetary embryos are distributed as suggested by *Bottke et al.* (2006) (Figs. 7 and 8). A compelling element to these runs is that they are consistent with the limited degree of semimajor axis mixing of large S- and C-type asteroids in the main belt (i.e., no exceptional process is needed here). Some key questions for this model, however, are whether planetary embryos ever existed in the asteroid belt, and if they did, how long they resided there before being dispersed by the formation and/or migration of Jupiter (see the chapter by Morbidelli et al. in this volume).

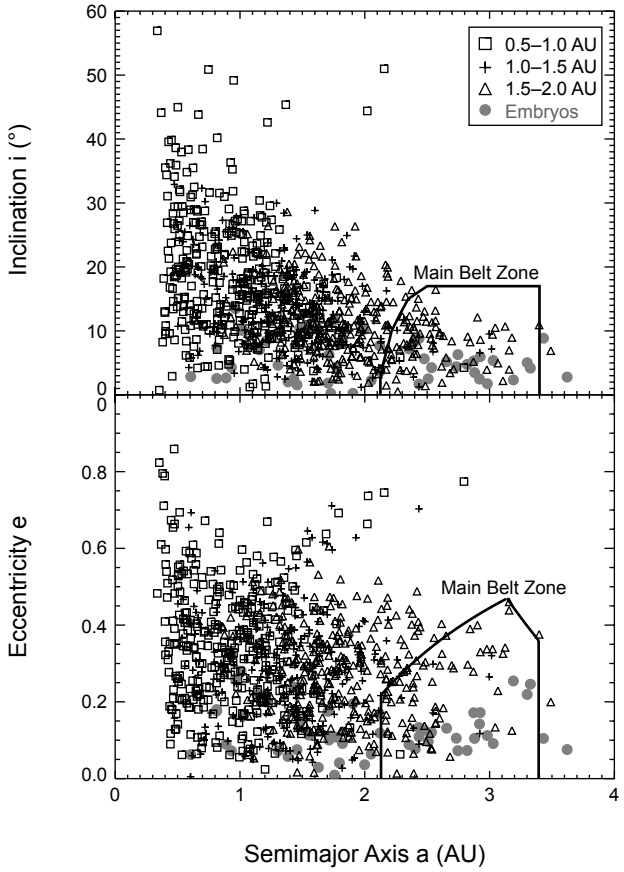

Fig. 7. Inclinations, eccentricities, and semimajor axes of planetesimals and planetary embryos in the inner solar system after 10 m.y. of dynamical evolution (*Bottke et al.,* 2006). The planetesimals were given uniform semimajor axis between 0.5 and 2.0 AU and low random eccentricities and inclinations. The squares, crosses, and triangles show what happens to 1000 planetesimals started with semimajor axes of 0.5–1.0 AU, 1.0–1.5 AU, and 1.5–2.0 AU, respectively. The black line shows the location of the main asteroid belt. Numerous planetary embryos, which are shown as gray dots, are distributed between 0.5 and 3.6 AU. We see that numerous planetesimals from different zones were driven into the main belt by gravitational interactions with planetary embryos. After *Bottke et al.* (2006).

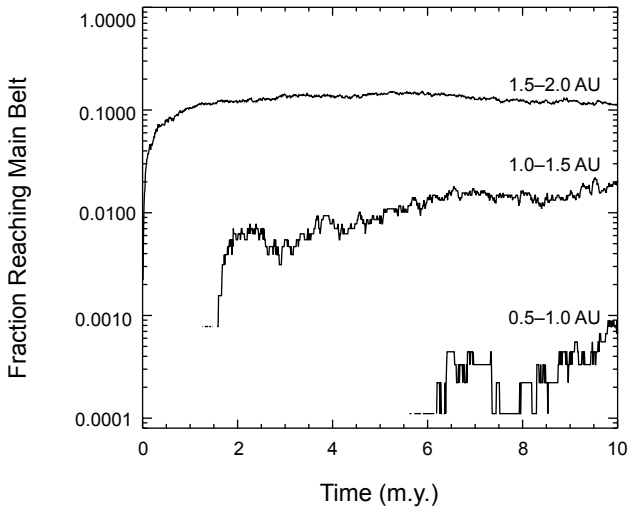

Fig. 8. The fraction of inner solar system planetesimals from 0.5–1.0 AU, 1.0–1.5 AU, and 1.5–2.0 AU scattered into the main belt by gravitational interactions with planetary embryos (see Fig. 7) (*Bottke et al.,* 2006). The largest proportion of test bodies reaching the main belt is from the adjacent 1.5–2.0-AU zone. For the 1.0–1.5-AU zone, 0.8–2% are injected into the main belt after a delay of 2 m.y., while for 0.5–1.0 AU we find that 0.01–0.1% enter after 6 m.y. This shows that material from the terrestrial planet region may be found in the main belt today. Key factors here are the existence of planetary embryos in all zones of interest and the formation time of Jupiter, which is assumed to have had a hand in eliminating embryos from the main belt. Note that giant planets are neglected in this model. After *Bottke et al.* (2006).

A second scenario involves scattering/capture opportunities within the so-called Grand Tack model, which assumes that Jupiter interacted with the nebular disk and migrated across the primordial asteroid belt within the first few million years of solar system history (*Walsh et al.,* 2011, 2012; see also the chapter by Morbidelli et al. in this volume). Here planetesimals and fragments from the terrestrial planet region would have had the opportunity to reach stable main-belt orbits via interactions with Jupiter. As Jupiter migrated inward across the asteroid belt, main-belt planetesimals would have been scattered onto highly eccentric orbits within the terrestrial planet region, mixing with planetesimals scattered by planetary embryos. When Jupiter turned around and migrated back outward toward its current orbit, many eccentric planetesimals would have been implanted in the main-belt zone, thereby providing a source for differentiated material. Jupiter's migration also implants planetesimals from the Jupiter-Saturn zone into the main-belt zone, where they potentially would make up the C-complex population. Finally, the Grand Tack model allows planetary embryos to reside in the primordial main belt prior to Jupiter's early migration. This means the implantation scenario discussed above would also be active until Jupiter scattered the planetary embryos out of the main-belt region.

A key question here is whether the implantation of differentiated material can be used to test the Grand Tack; too much material, or too little, could place constraints on this putative planet-formation mechanism. An addendum to this model would be to consider how much terrestrial planet material was placed into the main belt prior to the migration of Jupiter via the first scenario, which presumably took place a few million years after CAI formation.

In a third scenario, we present promising but preliminary work within the context of the Nice model (see the chapter by Morbidelli et al. in this volume). Here the giant planets were assumed to reside for hundreds of millions of years on nearly circular, coplanar orbits in a much more compact configuration than they have today (all between 5 and 12 AU). This not only means that their mean-motion resonances were

once in different locations than we see them today, but also that they once may have been stabilizing for objects trapped inside [e.g., Neptune's mean-motion resonances are stabilizing for Pluto and other resonant Kuiper belt objects (*Levison et al.,* 2008)]. This could also explain why primordial "Kirkwood gaps" associated with the original locations of the giant planets have not yet been found in the main-belt region. By simulating how planetary perturbations affected test bodies started outside the primordial main-belt region, we found that a small fraction of bodies scattering off Mars were able to enter into the primordial main belt on low-eccentricity, low-inclination orbits via "fossil" mean-motion resonances, where they stayed for hundreds of millions of years. These bodies become permanently captured when the host resonances moved during late giant planet migration.

An intriguing method to test this hypothesis may involve the M-type asteroids. Let us assume for the moment that the M-types are remnants of planetesimals that went through hit-and-run collisions, as discussed above. Thus we will assume that these bodies include both exposed core material [e.g., (16) Psyche] as well as core-enriched gravitational accumulations of leftover debris referred to as hodgepodge worlds [e.g., we speculate that (21) Lutetia might be an example]. Much of the other crust and mantle would have been pulverized or altered beyond recognition by the associated effects (i.e., hydrostatic unloading, shock, reduction, and depletion) and/or subsequent collisional evolution in the terrestrial planet region.

As described above, a few M-types might survive by finding a dynamical pathway onto stable orbits within the main-belt region. This could result from any of the three scenarios discussed above. The first two, gravitational scattering among planetary embryos (*Bottke et al.,* 2006) and the Grand Tack model, would predict that M-types should be distributed in modestly random fashion across the main belt, with perhaps the highest concentrations in the inner main belt near the adjacent terrestrial planet region. In contrast, the 26 M-types with diameter D > 50 km (see *Neese,* 2010) appear to be located at preferential values of semimajor axis a, and almost none are found in the inner main belt (Fig. 9). In addition, of the eight M-types with i < 5°, three are at a = 2.42 AU and four more are at a = 2.67 AU. None show signs of coming from a family-forming collision at either locale (i.e., no clustered orbits; no associated fragment size distributions).

These values instead suggest that the third scenario related to the Nice model may be the most preferable solution. To check this idea, we performed proof-of-concept simulations that track how these kinds of planetary perturbations affect test bodies approaching the primordial main-belt region (Fig. 9). Interestingly, for particles initially scattered off Mars, we found that a small but notable fraction not only entered into the primordial main belt via these "fossil" mean-motion resonances, but they also stayed there until the end of the simulation 300 m.y. later. Additional evidence for this scenario comes from the orbits of all our large M-type asteroids (Fig. 9). If we assume Jupiter was originally located at 5.55 AU prior to the onset of late giant planet migration, we can explain why many M-types are found near primordial jovian mean-motion resonances like the J3:1 (2.67 AU) and others in the central/outer main belt. The ones we cannot yet fit also show signs of promise (i.e., the J7:2 "stalactite" at 2.4 AU in Fig. 9 is close to the M-types there).

These results do not yet fit all the M-types, possibly because we lack the appropriate initial conditions for our captured asteroids as well as the starting orbits of the giant planets. Getting all the giant planets in the correct primordial configuration, while including effects like the possibility of lost giant planets (*Nesvorny,* 2011; *Nesvorny and Morbidelli,* 2012), will require a suite of careful and numerically expensive simulations.

In summary, we consider it plausible that some M-types, A types, V-types, and possibly other exotic asteroids were captured within the primordial main belt by the mechanisms discussed above. In fact, we cannot yet rule out the possibility that a large differentiated body like Vesta formed elsewhere as well, although we caution that low capture probabilities make it difficult to construct a compelling case for this idea at this time. Future studies of these scenarios, and any new ones that may arise, will be useful because they may eventually provide us with constraints on the timing and nature of planetesimal and planet formation as well as the initial orbits of the giant planets prior to early migration.

7. SUMMARY AND FUTURE WORK

Given the difficulties that conventional collisional processes have in explaining the differentiated meteorite record, our

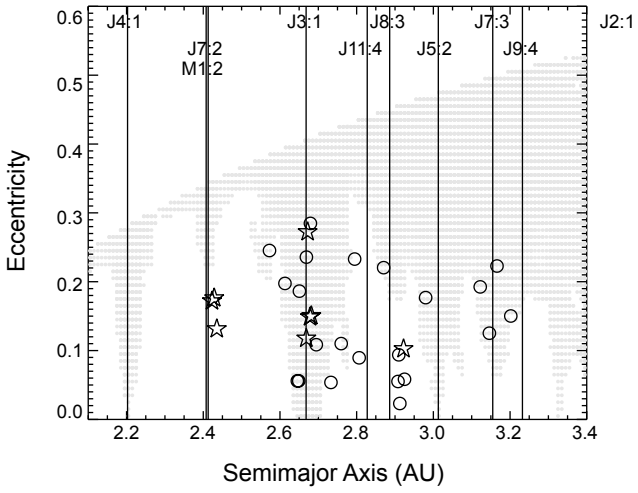

Fig. 9. M-type asteroids (D > 50 km) in the main belt are shown next to the putative primordial location of Jupiter's resonances. Here we assumed Jupiter's initial semimajor axis was 5.5 AU. The stars are M-types with i < 5°, and the circles are those with i > 5°. The gray dots show the orbits of scattered test bodies started in the terrestrial planet region that entered the main-belt zone with i < 20°. Some were captured on long-lived orbits within the putative locations of primordial dynamical resonances; this created the stalagmite-like features. Note that the match is interesting but imperfect, probably because the orbits of the giant planets are improperly positioned.

scenario for forming differentiated asteroids and meteorites by early accretion and disaggregation of melted planetesimals in the terrestrial planet region by hit-and-run impacts offers a new road map for explaining many of their anomalous properties and puzzling origin. In particular, it helps to explain why our collection of differentiated meteorites seems to resemble handfuls of pieces from numerous different jigsaw puzzles that cannot be reassembled into meaningful pictures. This scenario can be tested with detailed field work on differentiated asteroids by spacecraft, spectral studies of smaller asteroids, improved techniques for deriving mineral abundance and composition from spectra, better chronological constraints on the formation times of differentiated meteorites, and more detailed impact and dynamical models. We are optimistic that constraints from asteroids and meteorites can be used to discriminate between different dynamical models that have been proposed to account for the low mass of the asteroid belt and the small size of Mars (e.g., *Walsh et al.,* 2011, 2012).

We attribute much of the dunite shortage among meteorites and asteroids to preferential loss of mantle material from differentiated planetesimals by hit-and-run impacts during accretion. Mixing of molten metal and silicate by accretionary impacts may account for the formation of stony-iron meteorites, and their greater strength helps to explain the lack of complementary silicate. Silicate magma in differentiated planetesimals may also have been splashed out to form chondrules, as suggested by *Asphaug et al.* (2011) and *Sanders and Scott* (2012). Formation times of chondrules are well accounted for in this model, and chondrites, except CIs, are substantially depleted in Fe.

We have focused on one aspect of the origin and evolution of the asteroid belt during accretion but to make more progress we require a better understanding of the effects of impacts during subsequent epochs, viz., the formation of the Moon and the late heavy bombardment. We also need a better understanding of the impact history of chondrites. Did their parent bodies escape early disruption during accretion and metamorphism, as the onion-shell model requires (*Trieloff et al.,* 2003), or were they disrupted and disaggregated when hot like the differentiated planetesimals (*Ganguly et al.,* 2013; *Scott et al.,* 2014; *Van Niekerk et al.,* 2014)?

Acknowledgments. We thank numerous colleagues for helpful discussions and for sharing their insights and G. Consolmagno and D. O'Brien for helpful reviews. This research was supported by the NASA cosmochemistry program through grants NNX12AK68G (E.S.) and NN08AG53G and NNX11AF62G (J.I.G.). W.F.B was supported by NASA's Solar System Evolution Research Virtual Institute (SSERVI) program through a grant to the Institute for the Science of Exploration Targets at the Southwest Research Institute in Boulder, Colorado. Sadly, Joseph Goldstein passed away on June 27, 2015, before this book was published. We are grateful for his contribution to this chapter.

REFERENCES

Agnor C. and Asphaug E. (2004) Accretion efficiency during planetary collisions. *Astrophys. J. Lett., 613,* L157–L160.

Amelin Y., Ghosh A., and Rotenberg E. (2005) Unraveling the evolution of chondrite parent asteroids by precise U-Pb dating and thermal modeling. *Geochim. Cosmochim. Acta, 69,* 505–518.

Asphaug E. (2009) Growth and evolution of asteroids. *Annu. Rev. Earth Planet. Sci., 37,* 413–448.

Asphaug E. (2010) Similar-sized collisions and the diversity of planets. *Chem. Erde–Geochem., 70,* 199–219.

Asphaug E. and Reufer A. (2014) Mercury and other iron-rich planetary bodies as relics of inefficient accretion. *Nature Geosci., 7,* 564–568.

Asphaug E., Agnor C. B., and Williams Q. (2006) Hit and run planetary collisions. *Nature, 439,* 155–160.

Asphaug E., Jutzi M., and Movshovitz N. (2011) Chondrule formation during planetesimal accretion. *Earth Planet. Sci. Lett., 308,* 369–379.

Baker J. A., Schiller M., and Bizzarro M. (2012) ^{26}Al-^{26}Mg deficit dating ultramafic meteorites and silicate planetesimal differentiation in the early solar system? *Geochim. Cosmochim. Acta, 77,* 415–431.

Barucci M. A., Fornasier S., Dotto E., Lamy P. L., Jorda L., Groussin O., Brucato J. R., Carvano J., Alvarez-Candal A., Cruikshank D., and Fulchignoni M. (2008) Asteroids 2867 Steins and 21 Lutetia: Surface composition from far infrared observations with the Spitzer Space Telescope. *Astron. Astrophys., 477,* 665–670.

Barucci M. A., Belskaya I. N., Fornasier S., Fulchignoni M., Clark B. E., Coradini A., Capaccioni F., Dotto E., Birlan M., Leyrat C., Sierks H., Thomas N., and Vincent J. B. (2012) Overview of Lutetia's surface composition. *Planet. Space Sci., 66,* 23–30.

Bell J. F., Davis D. R., Hartmann W. K., and Gaffey M. J. (1989) Asteroids: The big picture. In *Asteroids II* (R. P. Binzel et al., eds.), pp. 921–945. Univ. of Arizona, Tucson.

Benedix G. K., Haack H., and McCoy T. J. (2014) Iron and stony-iron meteorites. In *Treatise on Geochemistry, Vol 1: Meteorites and Cosmochemical Processes, Second edition* (A. M. Davis, ed.), pp. 267–285. Elsevier, Oxford.

Binzel R. P. and Xu S. (1993) Chips off of asteroid 4 Vesta: Evidence for the parent body of basaltic achondrite meteorites. *Science, 260,* 186–191.

Bizzarro M., Baker J. A., Haack H., and Lundgaard K. L. (2005) Rapid timescales for accretion and melting of differentiated planetesimals inferred from ^{26}Al-^{26}Mg chronometry. *Astrophys. J., 632,* L41–L44.

Blichert-Toft J., Moynier F., Lee C.-T. A., Telouk P., and Albarede F. (2010) The early formation of the IVA iron meteorite parent body. *Earth Planet. Sci. Lett., 296,* 469–480.

Bogard D. D. (2011) K-Ar ages of meteorites: Clues to parent body thermal histories. *Chem. Erde–Geochem., 71,* 207–226.

Bogard D. D. and Garrison D. H. (2003) ^{39}Ar-^{40}Ar ages of eucrites and the thermal history of asteroid 4 Vesta. *Meteoritics & Planet. Sci., 38,* 669–710.

Bottke W. F. (2014) On the origin and evolution of Vesta and the V-type asteroids. In *Vesta in the Light of Dawn: First Exploration of a Protoplanet in the Asteroid Belt,* Abstract #2024. LPI Contrib. No. 1773, Lunar and Planetary Institute, Houston.

Bottke W. F., Nesvorny D., Grimm R. E., Morbidelli A., and O'Brien D. P. (2006) Iron meteorites as remnants of planetesimals formed in the terrestrial planet region. *Nature, 439,* 821–824.

Bottke W. F., Vokrouhlicky D., Minton D., Nesvorny D., Morbidelli A., Brasser R., Simonson B., and Levison H. F. (2012) An Archaean heavy bombardment from a destabilized extension of the asteroid belt. *Nature, 485,* 78–81.

Brennecka G. and Wadhwa M. (2012) Uranium isotope compositions of the basaltic angrite meteorites and the chronological implications for the early solar system. *Proc. Natl. Acad. Sci., 109,* 9299–9303.

Buchwald V. F. (1975) *Handbook of Iron Meteorites*. Univ. of California, Oakland. 1418 pp. Available online at *http://evols.library.manoa.hawaii.edu/handle/10524/33750*.

Burbine T. H. (2014) Asteroids. In *Treatise on Geochemistry, Vol. 2: Meteorites and Cosmochemical Processes, Second edition* (A. M. Davis, ed.), pp. 365–414. Elsevier, Oxford.

Burbine T. H., Meibom A., and Binzel R. P. (1996) Mantle material in the main belt: Battered to bits? *Meteoritics & Planet. Sci., 31,* 607–620.

Burbine T. H., Buchanan P. C., Binzel R. P., Bus S. J., Hiroi T., Hinrichs J. L., Meibom A., and McCoy T. J. (2001) Vesta, vestoids, and the howardite, eucrite, diogenite group: Relationships and the origin of spectral differences. *Meteoritics & Planet. Sci., 36,* 761–781.

Carruba V., Michtchenko T. A., Roig F., Ferraz-Mello S., and Nesvorny D. (2005) On the V-type asteroids outside the Vesta family I. Interplay of nonlinear secular resonances and the Yarkovsky

effect: The cases of 956 Elisa and 809 Lundia. *Astron. Astrophys., 441,* 819–829.
Carry B. (2012) Density of asteroids. *Planet. Space. Sci., 73,* 98–118.
Chambers J. E. (2013) Late-stage planetary accretion including hit-and-run collisions and fragmentation. *Icarus, 224,* 43–56.
Chabot N. L. (2004) Sulfur contents of the parental metallic cores of magmatic iron meteorites. *Geochim. Cosmochim. Acta, 68,* 3607–3618.
Chapman C. R. (1986) Implications of the inferred compositions of asteroids for their collisional evolution. *Mem. Soc. Astron. Ital., 57,* 103–114.
Ciesla F. J., Davison T. M., Collins G. S., and O'Brien D. P. (2013) Thermal consequences of impacts in the early solar system. *Meteoritics & Planet. Sci., 48,* 2559–2576.
Clark B. E., Bus S. J., Rivkin A. S., Shepard M. K., and Shah S. (2004) Spectroscopy of X-type asteroids. *Astron. J., 128,* 3070–3081.
Clark B. E., Ockert-Bell M. E., Cloutis E. A., Nesvorny D., Mothe-Diniz T., and Bus S. J. (2009) Spectroscopy of K-complex asteroids: Parent bodies of carbonaceous meteorites? *Icarus, 202,* 119–133.
Cloutis E. A., Binzel R. P., Burbine T. H., Gaffey M. J., and McCoy T. J. (2006) Asteroid 3628 Boznemcova: Covered with angrite-like basalts? *Meteoritics & Planet. Sci., 41,* 1147–1161.
Connelly J. N., Bizzarro M., Krot A. N., Norlund A., Wielendt D., and Ivanova M. (2012) The absolute chronology and thermal processing of solids in the solar protoplanetary disk. *Science, 338,* 651–655.
Consolmagno G. J. and Drake M. J. (1977) Composition and evolution of the eucrite parent body: Evidence from rare earth elements. *Geochim. Cosmochim. Acta, 41,* 1271–1282.
Consolmagno G. J., Golabeck G., Turrini D., Jutzi M., Sirono S., Svetsov V., and Tsiganis K. (2014) Is Vesta an intact and pristine protoplanet? *Icarus, 254,* 190–201.
Cruikshank D. P., Tholen D. J., Hartmann W. K., Bell J. F., and Brown R. H. (1991) Three basaltic Earth-approaching asteroids and the source of the basaltic meteorites. *Icarus, 89,* 1–13.
Dale C. W., Burton K. W., Greenwood R. C., Gannoun A., Wade J., Wood B. J., and Pearson D. G. (2012) Late accretion on the earliest planetesimals revealed by the highly siderophile elements. *Science, 336,* 72–75.
Davis A. M. and McKeegan K. D. (2014) Short-lived radionuclides and early solar system chronology. In *Treatise on Geochemistry, Vol. 1: Meteorites and Cosmochemical Processes, Second edition* (A. M. Davis, ed.), pp. 361–395, Elsevier, Oxford.
Davis D. R., Chapman C. R., Weidenschilling S. J., and Greenberg R. (1985) Collisional history of asteroids — Evidence from Vesta and the Hirayama families. *Icarus, 62,* 30–53.
Davis D. R., Farinella P., and Marzari F. (1999) The missing Psyche family: Collisionally eroded or never formed? *Icarus, 137,* 140–151.
Davison T. M., Ciesla F. J., and Collins G. S. (2012) Post-impact thermal evolution of porous planetesimals. *Geochim. Cosmochim. Acta, 95,* 252–269.
Davison T. M., O'Brien D. P., Ciesla F. J., and Collins G. S. (2013) The early impact histories of meteorite parent bodies. *Meteoritics & Planet. Sci., 48,* 1894–1918.
Delbo M., Gai M., Lattanzi M. G., Ligori S., Loreggia D., Saba L., Cellino A., Gandolfi D., Licchelli D., Blanco C., Cigna M., and Wittkowski M. (2006) MIDI observations of 1459 Magnya: First attempt of interferometric observations of asteroids with the VLTI. *Icarus, 181,* 618–622.
DeMeo F. E. and Carry B. (2013) The taxonomic distribution of asteroids from multi-filter all-sky photometric surveys. *Icarus, 226,* 723–741.
DeMeo F. E. and Carry B. (2014) Solar system evolution from compositional mapping of the asteroid belt. *Nature, 505,* 629–634.
DeMeo F. E., Binzel R. P., Slivan S. M., and Bus S. J. (2009) An extension of the Bus asteroid taxonomy into the near-infrared. *Icarus, 202,* 160–180.
De Sanctis M. C., Ammannito E., Migliorini A., Lazzaro D., Capria M. T., and McFadden L. (2011) Mineralogical characterization of some V-type asteroids, in support of the NASA Dawn mission. *Mon. Not. R. Astron. Soc., 412,* 2318–2332.
Descamps P., Marchis F., Berthier J., Emery J. P., Duchene G., de Pater I., Wong M. H., Lim L., Hammel H. B., Vachier F., Wiggins P., Teng-Chuen-Yu J.-P., Peyrot A., Pollock J., Assafin M., Vieira-Martins R., Camargo J. I. B., Braga-Ribas F., and Macomber B. (2011) Triplicity and physical characteristics of asteroid (216) Kleopatra. *Icarus, 211,* 1022–1033.
D'Orazio M., Folco L., Chaussidon M., and Rochette P. (2009) Sahara 03505 sulfide-rich iron meteorite: Evidence for efficient segregation of sulfide-rich metallic melt during high-degree impact melting of an ordinary chondrite. *Meteoritics & Planet. Sci., 44,* 221–231.
Duffard R. and Roig F. (2009) Two new V-type asteroids in the outer main belt? *Planet. Space Sci., 57,* 229–234.
Duffard R., Lazzaro D., Licandro J., De Sanctis M. C., Capria M. T., and Carvano J. M. (2004) Mineralogical characterization of some basaltic asteroids in the neighborhood of (4) Vesta: First results. *Icarus, 171,* 120–132.
Farquhar R., Kawaguchi J. Russell C. T., Schwehm G., Veverja J., and Yeomans D. (2002) Spacecraft exploration of asteroids: The 2001 perspective. In *Asteroids III* (W. F. Bottke Jr. et al., eds.), pp. 367–376. Univ. of Arizona, Tucson.
Fieber-Beyer S. K., Gaffey M. J., and Abell P. A. (2011a) Mineralogical characterization of near-Earth asteroid (1036) Ganymed. *Icarus, 212,* 149–157.
Fieber-Beyer S. K., Gaffey M. J., Kelley M. S., Reddy V., Reynolds C. M., and Hicks T. (2011b) The Maria asteroid family: Genetic relationships and a plausible source of mesosiderites near the 3:1 Kirkwood gap. *Icarus, 213,* 524–537.
Ganguly J. and Tirone M. (2001) Relationship between cooling rate and cooling age of a mineral: Theory and application to meteorites. *Meteoritics & Planet. Sci., 36,* 167–175.
Ganguly J., Tirone M., Chakraborty S., and Domanik K. (2013) H-chondrite parent asteroid: A multistage cooling, fragmentation and re-accretion history constrained by thermometric studies, diffusion kinetic modeling, and geochronological data. *Geochim. Cosmochim. Acta, 105,* 206–220.
Golabek G. J., Bourdon B., and Gerya T. V. (2014) Numerical models of the thermomechanical evolution of planetesimals: Application to the acapulcoite-lodranite parent body. *Meteoritics & Planet. Sci., 49,* 1083–1099.
Goldstein J. I., Scott E. R. D., and Chabot N. L. (2009) Iron meteorites: Crystallization, thermal history, parent bodies, and origin. *Chem. Erde–Geochem, 69,* 293–325.
Goldstein J. I., Yang J., and Scott E. R. D. (2014) Determining cooling rates of iron and stony-iron meteorites from measurements of Ni and Co at kamacite-taenite interfaces. *Geochim. Cosmochim. Acta, 140,* 297–320.
Goodrich C. A., Scott E. R. D., and Fioretti A. M. (2004) Ureilitic breccias: Clues to the petrologic structure and impact disruption of the ureilite parent asteroid. *Chem. Erde–Geochem., 64,* 283–327.
Goodrich C. A., Hutcheon I. D., Kita N. T., Huss G. R., Cohen B. A., and Keil K. (2010) ^{53}Mn-^{53}Cr and ^{26}Al-^{26}Mg ages of a feldspathic lithology in polymict ureilites. *Earth Planet. Sci. Lett., 295,* 531–540.
Goodrich C. A., Hartmann W. K., O'Brien D. P., Weidenschilling S. J., Wilson L., Michel P., and Jutzi M. (2015) Origin and history of ureilitic material in the solar system: The view from asteroid 2008 TC_3 and the Almahata Sitta meteorite. *Meteoritics & Planet. Sci., 50,* 782–809.
Göpel C. and Manhes G. (2010) The thermal history of the Acapulco meteorite and its parent body deduced from U/Pb systematics in mineral separates and bulk rock fragments. *Compt. Rend. Geosci., 342,* 53–59.
Greenwood R. C., Franchi I. A., Gibson J. M., and Benedix G. K. (2012) Oxygen isotope variation in primitive achondrites: The influence of primordial, asteroidal, and terrestrial processes. *Geochim. Cosmochim. Acta, 94,* 146–163.
Haack H., Scott E. R. D., Love S. G., Brearley A. J., and McCoy T. J. (1996) Thermal histories of IVA stony-iron and iron meteorites: Evidence for asteroid fragmentation and reaccretion. *Geochim. Cosmochim. Acta, 60,* 3103–3113.
Hardersen P. S., Gaffey M. J., and Abell P. A. (2004) Mineralogy of asteroid 1459 Magnya and implications for its origin. *Icarus, 167,* 170–177.
Herzog G. F. and Caffee M. W. (2014) Cosmic-ray exposure ages of meteorites. In *Treatise on Geochemistry, Vol. 1: Meteorites and Cosmochemical Processes, Second edition* (A. M. Davis, ed.), pp. 419–453. Elsevier, Oxford.
Hevey P. J. and Sanders I. S. (2006) A model for planetesimal meltdown by ^{26}Al and its implications for meteorite parent bodies. *Meteoritics & Planet. Sci., 41,* 95–106.
Hiroi T. and Sasaki S. (2001) Importance of space weathering simulation products in compositional modeling of asteroids: 349 Dembowska

and 446 Aeternitas as examples. *Meteoritics & Planet. Sci., 36,* 1587–1596.
Keil K. (2002) Geological history of asteroid 4 Vesta: The "smallest terrestrial planet." In *Asteroids III* (W. F. Bottke Jr. et al., eds.), pp. 573–584. Univ. of Arizona, Tucson.
Keil K. (2010) Enstatite achondrite meteorites (aubrites) and the histories of their asteroidal parent bodies. *Chem. Erde–Geochem., 70,* 295–317.
Keil K. (2011) Angrites, a small but diverse suite of ancient, silica-undersaturated volcanic-plutonic mafic meteorites, and the history of their parent asteroid. *Chem. Erde–Geochem., 72,* 191–218.
Keil K. (2014) Brachinite meteorites: Partial melt residues from an FeO-rich asteroid. *Chem. Erde–Geochem., 74,* 311–329.
Keil K., Ntaflos Th., Taylor G. J., Brearley A. J., and Newsom H. E. (1989) The Shallowater aubrite — Evidence for origin by planetesimal impacts. *Geochim. Cosmochim. Acta, 53,* 3291–3307.
Keil K., Haack H., and Scott E. R. D. (1994) Catastrophic fragmentation of asteroids: Evidence from meteorites. *Planet. Space Sci., 42,* 1109–1122.
Keil K., Stöffler D., Love S. G., and Scott E. R. D. (1997) Constraints on the role of impact heating and melting in asteroids. *Meteoritics & Planet. Sci., 32,* 349–363.
Kita N. T. and Ushikubo T. (2012) Evolution of protoplanetary disk inferred from ^{26}Al chronology of individual chondrules. *Meteoritics & Planet. Sci., 47,* 1108–1119.
Kleine T., Mezger K., Palme H., Scherer E., and Münker C. (2005) Early core formation in asteroids and late accretion of chondrite parent bodies: Evidence from ^{182}Hf-^{182}W in CAIs, metal-rich chondrites, and iron meteorites. *Geochim. Cosmochim. Acta, 69,* 5805–5818.
Kleine T., Touboul M., Van Orman J. A., Bourdon B., Maden C., Mezger K., and Halliday A. N. (2008) Hf-W thermochronometry: Closure temperature and constraints on the accretion and cooling history of the H chondrite parent body. *Earth Planet. Sci. Lett., 270,* 106–118.
Kleine T., Hans U., Irving A. J., and Bourdon B. (2012) Chronology of the angrite parent body and implications for core formation in protoplanets. *Geochim. Cosmochim. Acta, 84,* 186–203.
Kleine T., Hans U., Irving A. J., and Bourdon B. (2013) Chronology of the angrite parent body and implications for core formation in protoplanets. *Geochim. Cosmochim. Acta, 84,* 186–203.
Kring D. A., Hill D. H., Gleason J. D., Britt D. T., Consolmagno G. J., Farmer M., Wilson S., and Haag R. (1999) Portales Valley: A meteoritic sample of the brecciated and metal-veined floor of an impact crater on an H-chondrite asteroid. *Meteoritics & Planet. Sci., 34,* 663–669.
Krot A. N., Amelin Y., Cassen P., and Meibom A. (2005) Young chondrules in CB chondrites from a giant impact in the early solar system. *Nature, 436,* 989–992.
Krot A. N., Nagashima K, Yoshitake M., and Yurimoto H. (2010) Oxygen isotopic compositions of chondrules from the metal-rich chondrites Isheyevo (CH/CB$_b$), MAC 02675 (CB$_b$) and QUE 94627 (CB$_b$). *Geochim. Cosmochim. Acta, 74,* 2190–2211.
Krot A. N., Makide K., Nagashima K., Huss G. R., Ogliore R. C., Ciesla F. J., Yang L., Hellebrand E., and Gaidos E. (2012) Heterogeneous distribution of ^{26}Al at the birth of the solar system: Evidence from refractory grains and inclusions. *Meteoritics & Planet. Sci., 47,* 1848–1979.
Krot A. N., Keil K., Scott E. R. D., Goodrich C. A., and Weisberg M. K. (2014) Classification of meteorites and their genetic relationships. In *Treatise on Geochemistry, Vol. 1: Meteorites and Cosmochemical Processes, Second edition* (A. M. Davis, ed.), pp. 1–63. Elsevier, Oxford.
Kruijer T. S., Sprung P., Kleine T., Leya I., Burkhardt C., and Wieler R. (2012) Hf-W chronometry of core formation in planetesimals inferred from weakly irradiated iron meteorites. *Geochim. Cosmochim. Acta, 99,* 287–304.
Kruijer T. S., Fischer-Gödde M., Kleine T., Sprung P., Leya I., and Wieler R. (2013) Neutron capture on Pt isotopes in iron meteorites and the Hf-W chronology of core formation in planetesimals. *Earth Planet. Sci. Lett., 361,* 162–172.
Kruijer T. S., Kleine T., Fischer-Gödde M., Burkhardt C., and Wieler R. (2014) Nucleosynthetic W isotopic anomalies and the Hf-W chronometry of Ca-Al-rich inclusions. *Earth Planet. Sci. Lett., 403,* 317–327.
Lazzaro D., Michtchenki T., Carvano J. M., Binzel R. P., Bus S. J., Burbine T. H., Mothe-Diniz T., Florczak M., Angeli C. A., and Harris A. W. (2000) Discovery of a basaltic asteroid in the outer main belt. *Science, 288,* 2033–2035.
Levison H., Morbidelli A., VanLaerhoven C., Gomes R., and Tsiganis K. (2008) Origin of the structure of the Kuiper belt during a dynamical instability in the orbits of Uranus and Neptune. *Icarus, 196,* 258–273.
Lugmair G. W. and Shukolyukov A. (1998) Early solar system timescales according to ^{53}Mn-^{53}Cr systematics. *Geochim. Cosmochim. Acta, 62,* 2863–2886.
Marchi S. and 11 colleagues (2012) The violent collisional history of asteroid 4 Vesta. *Science, 336,* 690–694.
Marchi S. and 10 colleagues (2013) High-velocity collisions from the lunar cataclysm recorded in asteroidal meteorites. *Nature Geosci., 6,* 303–307.
Marsh C. A., Della-Giustina D. N., Giacalone J., and Lauretta D. S. (2006) Experimental tests of the induction heating hypothesis for planetesimals. *Lunar Planet. Sci. XXXVII,* Abstract #2078. Lunar and Planetary Institute, Houston.
Masiero J. R. and 17 colleagues (2011) Main belt asteroids with WISE/NEOWISE. I. Preliminary albedos and diameters. *Astrophys. J., 741,* 68.
Masiero J. R., Mainzer A. K., Bauer J. M., Grav T., Nugent C. R., and Stevenson R. (2013) Asteroid family identification using the hierarchical clustering method and WISE/NEOWISE physical properties. *Astrophys. J., 770,* 22.
Mayne R. G., Sunshine J. M., McSween H. Y. Jr., Bus S. J., and McCoy T. J. (2011) The origin of Vesta's crust: Insight from spectroscopy of the vestoids. *Icarus, 214,* 147–160.
McCord T. B., Adams J. B., and Johnson T. V. (1970) Asteroid Vesta: Spectral reflectivity and compositional implications. *Science, 168,* 1445–1447.
McCoy T. J. and 9 colleagues (1996) A petrologic, chemical, and isotopic study of Monument Draw and comparison with other acapulcoites: Evidence for formation by incipient partial melting. *Meteoritics & Planet. Sci., 60,* 2682–2708.
McCoy T. J., Keil K., Clayton R. N., Mayeda T. K., Bogard D. D., Garrison D. H., and Wieler R. (1997) A petrologic and isotopic study of lodranites: Evidence for early formation as partial melt residues from heterogeneous precursors. *Geochim. Cosmochim. Acta, 61,* 623–637.
McSween H. Y. and 11 colleagues (2013) Dawn; the Vesta-HED connection; and the geologic context for eucrites, diogenites, and howardites. *Meteoritics & Planet. Sci., 48,* 2090–2104.
Mikouchi T., Zolensky M. E., Ohnishi I., Suzuki T., Takeda H., Jenniskens P., and Shaddad M. H. (2010) Electron microscopy of pyroxene in the Almahata Sitta ureilite. *Meteoritics & Planet. Sci., 45,* 1812–1820.
Michel P., Benz W., and Richardson D. C. (2004) Catastrophic disruption of pre-shattered parent bodies. *Icarus, 168,* 420–432.
Milani A., Knezevic Z., Novakovic B., and Cellino A. (2010) Dynamics of the Hungaria asteroids. *Icarus, 207,* 769–794.
Mittlefehldt D. W. (2005) Ibitira: A basaltic achondrite from a distinct parent asteroid and implications for the Dawn mission. *Meteoritics & Planet. Sci., 46,* 665–677.
Morbidelli A., Bottke W. F., Nesvorný D., and Levison H. F. (2009) Asteroids were born big. *Icarus, 204,* 558–573.
Moskovitz N. A. and Gaidos E. (2009) Differentiation of planetesimals and the thermal consequences of melt migration. *Meteoritics & Planet. Sci., 46,* 903–918.
Moskovitz N. A., Lawrence S., Jedicke R., Willman M., Haghighipour N., Bus S. J., and Gaidos E. (2008) A spectroscopically unique main-belt asteroid: 10537 (1991 RY16). *Astrophys. J., 682,* L57–L60.
Moskovitz N. A., Willman M., Burbine T. H., Binzel R. P., and Bus S. J. (2010) A spectroscopic comparison of HED meteorites and V-type asteroids in the inner main belt. *Icarus, 208,* 773–788.
Mothe-Diniz T. and Carvano J. M. (2005) 221 Eos: A remnant of a partially differentiated parent body? *Astron. Astrophys., 442,* 727–729.
Mothe-Diniz T., Carvano J. M., Bus S. J., Duffard R., and Burbine T. H. (2008) Mineralogical analysis of the Eos family from near-infrared spectra. *Icarus, 195,* 277–294.
Nathues A. (2010) Spectral study of the Eunomia asteroid family. Part II: The small bodies. *Icarus, 208,* 252–275.
Nathues A., Mottola S., Kaasalainen M., and Neukum G. (2005) Spectral study of the Eunomia asteroid family. I. Eunomia. *Icarus, 175,* 452–463.
Neese C., ed. (2010) *Asteroid Taxonomy V6.0.* EAR-A-5-DDR-TAXONOMY-V6.0, NASA Planetary Data System.

Neeley J. R., Clark B. E., Ockert-Bell M. E., Shepard M. K., Conklin J., Cloutis E. A., Fornasier F., and Bus S. J. (2014) The composition of M-type asteroids II: Synthesis of spectroscopic and radar observations. *Icarus, 238,* 37–50.

Nesvorny D. (2011) Young solar system's fifth giant planet? *Astrophys. J. Lett., 742,* L22.

Nesvorny D. and Morbidelli A. (2012) Statistical study of the early solar system's instability with four, five, and six giant planets. *Astrophys. J., 144,* 117.

Nesvorny D., Roig F., Gladman B., Lazzaro D., Carruba V., and Mothe-Diniz T. (2008) Fugitives from the Vesta family. *Icarus, 193,* 85–95.

Neumann W., Breuer D., and Spohn T. (2012) Differentiation and core formation in accreting planetesimals. *Astron. Astrophys., 543,* A141.

O'Brien D. P., Morbidelli A., and Levison H. F. (2006) Terrestrial planet formation with strong dynamical friction. *Icarus, 184,* 39–58.

Ockert-Bell M. E., Clark B. E., Shepard M. K., Isaacs R. A., Cloutis E. A., Fornasier F., and Bus S. J. (2010) The composition of M-type asteroids: Synthesis of spectroscopic and radar observations. *Icarus, 210,* 674–692.

Petaev M. I., Clarke R. S. Jr., Jarosewich E., et al. (2000) The Chaunskij anomalous mesosiderite: Petrology, chemistry, oxygen isotopes, classification, and origin. *Geochem. Intl., 38,* S322–S350.

Petit J. M., Chambers J., Franklin F., and Nagasawa M. (2002) Primordial excitation and depletion of the main belt. In *Asteroids III* (W. F. Bottke Jr. et al., eds.), pp. 711–723. Univ. of Arizona, Tucson.

Reufer A., Meier M. M. M., Benz W., and Wieler R. (2012) A hit-and-run giant impact scenario. *Icarus, 221,* 296–299.

Rivkin A. S., Howell E. S., Lebofsky L. A., Clark B. E., and Britt D. T. (2000) The nature of M-class asteroids from 3 micron observations. *Icarus, 145,* 351–368.

Roig F., Nesvorny D., Gil-Hutton R., and Lazzaro D. (2008) V-type asteroids in the middle main belt. *Icarus, 194,* 125–136.

Rubin A. E., Ulff-Møller F., Wasson J. T., and Carlson W. D. (2001) The Portales Valley meteorite breccia: Evidence for impact-induced melting and metamorphism of an ordinary chondrite. *Geochim. Cosmochim. Acta, 65,* 323–342.

Ruzicka A. (2014) Silicate-bearing iron meteorites and their implications for the evolution of asteroidal parent bodies. *Chem. Erde–Geochem, 74,* 3–48.

Safronov V. S. (1972) *Evolution of the Protoplanetary Cloud and Formation of the Earth and Planets.* NASA TM F-677, Washington, DC.

Sanborn M. E. and Yin Q. Z. (2014) Chromium isotopic composition of the anomalous eucrites: An additional geochemical parameter for evaluating their origin. *Lunar Planet. Sci. XLV,* Abstract #2018. Lunar and Planetary Institute, Houston.

Sanchez J. A., Reddy V., Kelley M. S., Cloutis E. A., Bottke W. F., Nesvorny D., Lucas M. P., Hardersen P. S., Gaffey M. J., Abell P. A., and Le Corre L. (2014) Olivine-dominated asteroids: Mineralogy and origin. *Icarus, 228,* 288–300.

Sanders I. S. and Scott E. R. D. (2012) The origin of chondrules and chondrites: Debris from low-velocity impacts between molten planetesimals. *Meteoritics & Planet. Sci., 47,* 2170–2192.

Schulz T., Upadhyay D., Münker C., and Mezger K. (2012) Formation and exposure history of non-magmatic iron meteorites and winonaites: Clues from Sm and W isotopes. *Geochim. Cosmochim. Acta, 85,* 200–212.

Scott E. R. D. and Bottke W. F. (2011) Impact histories of angrites, eucrites, and their parent bodies. *Meteoritics & Planet. Sci., 46,* 1878–1887.

Scott E. R. D., Greenwood R. C., Franchi I. A., and Sanders I. S. (2009) Oxygen isotopic constraints on the origin and parent bodies of eucrites, diogenites, and howardites. *Geochim. Cosmochim. Acta, 73,* 5835–5853.

Scott E. R. D., Krot T. V., Goldstein J. I., and Wakita S. (2014) Thermal and impact history of the H chondrite parent asteroid during metamorphism: Constraints from metallic Fe-Ni. *Geochim. Cosmochim. Acta, 136,* 13–37.

Shepard M. K., Kressler K. M., Clark B. E., Ockert-Bell M., Nolan M. C., Howell E. S., Magri C., Giorgini J. D., Benner L. A. M., and Ostro S. J. (2008) Radar observations of E-class asteroids 44 Nysa and 434 Hungaria. *Icarus, 195,* 220–225.

Shepard M. K., Clark B. E., Ockert-Bell M., Nolan M. C., Howell E. S., Magri C., Giorgini J. D., Benner L. A. M., Ostro S. J., Harris A. W., Warner B. D., Stephens R. D., and Mueller M. (2010) A radar survey of M- and X-class asteroids. II. Summary and synthesis. *Icarus, 208,* 221–237.

Solontoi M. R., Hammergren M., Gyuk G., and Puckett A. (2012) AVAST survey 0.4–1.0 micron spectroscopy of igneous asteroids in the inner and middle main belt. *Icarus, 220,* 577–585.

Stewart B. W., Papanastassiou D. A., and Wasserburg G. J. (1994) Sm-Nd chronology and petrogenesis of mesosiderites. *Geochim. Cosmochim. Acta, 58,* 3487–3509.

Stewart S. T. and Leinhardt Z. M. (2012) Collisions between gravity-dominated bodies. II. The diversity of impact outcomes during the end stage of planet formation. *Astrophys. J., 751,* 32.

Sugiura N. and Fujiya W. (2014) Correlated accretion ages and ε^{54}Cr of meteorite parent bodies and the evolution of the solar nebula. *Meteoritics & Planet. Sci., 49,* 1–16.

Sugiura N. and Hoshino H. (2003) Mn-Cr chronology of five IIIAB iron meteorites. *Meteoritics & Planet. Sci., 38,* 117–143.

Sunshine J. M., Bus S. J., McCoy T. J., Burbine T. H., Corrigan C. M., and Binzel R. P. (2004) High-calcium pyroxene as an indicator of igneous differentiation in asteroids and meteorites. *Meteoritics & Planet. Sci., 39,* 1343–1357.

Sunshine J. M., Bus S. J., Corrigan C. M., McCoy T. J., and Burbine T. H. (2007) Olivine-dominated asteroids and meteorites: Distinguishing nebular and igneous histories. *Meteoritics & Planet. Sci., 42,* 155–170.

Tang H. and Dauphas N. (2012) Abundance, distribution, and origin of ^{60}Fe in the solar protoplanetary disk. *Earth Planet. Sci. Lett., 359–360,* 248–263.

Tarduno J. A., Cottrell R. D., Nimmo F., Hopkins J., Voronov J., Erickson A., Blackman E., Scott E. R. D., and McKinley R. (2012) Evidence for a dynamo in the main group pallasite parent body. *Science, 338,* 939–942.

Theis K. J., Schönbächler M., Benedix G. K., Rehkämper M., Andreasen R., and Davies C. (2013) Palladium-silver chronology of IAB iron meteorites. *Earth Planet. Sci. Lett., 361,* 402–411.

Tholen D. J. (1984) Asteroid taxonomy from cluster analysis of photometry. Ph.D. thesis, Univ. of Arizona, Tucson.

Trieloff M., Jessberger E. K., Herrwerth I., Hopp J., Fiéni C., Ghélis M., Bourot-Denise M., and Pellas P. (2003) Structure and thermal history of the H-chondrite parent asteroid revealed by thermochronometry. *Nature, 422,* 502–506.

Van Niekerk D., Scott E. R. D., and Taylor G. J. (2014) Constraints on the thermal and impact history of ordinary chondrites from two-pyroxene equilibration temperatures. *Lunar Planet. Sci. XLV,* Abstract #2374. Lunar and Planetary Institute, Houston.

Vernazza P., Brunetto R., Binzel R. P., Perron C., Fulvio D., Strazzulla G., and Fulchignoni M. (2009) Plausible parent bodies for enstatite chondrites and mesosiderites: Implications for Lutetia's fly-by. *Icarus, 202,* 477–486.

Vernazza P., Zanda B., Binzel R. P., Hiroi T., DeMeo F. E., Birlan M., Hewins R., Ricci L., Barge P., and Lockhart M. (2014) Multiple and fast: The accretion of ordinary chondrite parent bodies. *Astrophys. J., 791,* 120.

Vogel N. and Renne P. R. (2008) ^{40}Ar-^{39}Ar dating of plagioclase grain size separates from silicate inclusions in IAB iron meteorites and implications for the thermochronological evolution of the IAB parent body. *Geochim. Cosmochim. Acta, 72,* 1231–1255.

Wadhwa M. (2014) Solar system timescales from long-lived radioisotopes in meteorites and planetary materials. In *Treatise on Geochemistry, Vol. 1: Meteorites and Cosmochemical Processes, Second edition* (A. M. Davis, ed.), pp. 397–418. Elsevier, Oxford.

Wadhwa M., Amelin Y., Bogdanovski O., Shukolyukov A., Lugmair G. W., and Janney P. (2009) Ancient relative and absolute ages for a basaltic meteorite: Implications for timescales for planetary accretion. *Geochim. Cosmochim. Acta, 73,* 5189–5201.

Walsh K. J., Morbidelli A., Raymond S. N., O'Brien D. P., and Mandell A. M. (2011) A low mass for Mars from Jupiter's early gas-driven migration. *Nature, 475,* 206–209.

Walsh K. J., Morbidelli A., Raymond S. N., O'Brien D. P., and Mandell A. M. (2012) Populating the asteroid belt from two parent source regions due to the migration of giant planets — "The Grand Tack." *Meteoritics & Planet. Sci., 47,* 1941–1947.

Warner B. D., Harris A. W., Vokrouhlicky D., Nesvorny D., and Bottke W. F. (2009) Analysis of the Hungaria asteroid population. *Icarus, 204,* 172–182.

Wasson J. T. (2011) Relationship between iron-meteorite composition and size: Compositional distribution of irons from North Africa. *Geochim. Cosmochim. Acta, 75,* 1757–1772.

Wasson J. T. and Hoppe P. (2012) Co/Ni ratios at taenite/kamacite interfaces and relative cooling rates in iron meteorites. *Geochim. Cosmochim. Acta, 84,* 508–524.

Wasson J. T. and Kallemeyn G. W. (2002) The IAB iron-meteorite complex: A group, five subgroups, numerous grouplets, closely related, mainly formed by crystal segregation in rapidly cooling melts. *Geochim. Cosmochim. Acta, 66,* 2445–2473.

Weidenschilling S. J. and Cuzzi J. N. (2006) Accretion dynamics and timescales: Relation to chondrites. In *Meteorites and the Early Solar System II* (D. S. Lauretta and H. Y. McSween Jr., eds.), pp. 473–485. Univ. of Arizona, Tucson.

Weiss B. P. and Elkins-Tanton L. T. (2013) Differentiated planetesimals and the parent bodies of chondrites. *Annu. Rev. Earth Planet. Sci., 41,* 529–560.

Weiss B. P., Berdahl A. S., Elkins-Tanton L. T., Stanley S., Lima E. A., and Carporzen L. (2008) Magnetism on the angrite parent body and the early differentiation of planetesimals. *Science, 322,* 713–716.

Weiss B. P. and 12 coauthors (2012) Possible evidence for partial differentiation of asteroid Lutetia from Rosetta. *Planet. Space Sci., 66,* 137–146.

Wetherill G. W. (1980) Formation of the terrestrial planets. *Annu. Rev. Astron. Astrophys., 18,* 77–113.

Wilson L. and Keil K. (1991) Consequences of explosive eruptions on small solar system bodies: The case of the missing basalts on the aubrite parent body. *Earth Planet. Sci. Lett., 104,* 505–512.

Yang J. and Goldstein J. I. (2006) Metallographic cooling rates of the IIIAB iron meteorites. *Geochim. Cosmochim. Acta, 70,* 3197–3215.

Yang J., Goldstein J. I., and Scott E. R. D. (2007) Iron meteorite evidence for early formation and catastrophic disruption of protoplanets. *Nature, 446,* 888–891.

Yang J., Goldstein J. I., and Scott E. R. D. (2008) Metallographic cooling rates and origin of IVA iron meteorites. *Geochim. Cosmochim. Acta, 72,* 3043–3061.

Yang J., Goldstein J. I. and Scott E. R. D. (2010a) Main-group pallasites: Thermal history, relationship to IIIAB irons, and origin. *Geochim. Cosmochim. Acta, 74,* 4471–4492.

Yang J., Goldstein J. I., Michael J. R., Kotula P. G. and Scott E. R. D. (2010b) Thermal history and origin of the IVB iron meteorites and their parent body. *Geochim. Cosmochim. Acta, 74,* 4493–4506.